Endosomal actin branching, fission, and receptor recycling require FCHSD2 recruitment by MICAL-L1

Frisby, Devin; Murakonda, Ajay B.; Ashraf, Bazella; Dhawan, Kanika; Almeida-Souza, Leonardo ...

2024-11-01
AMERICAN SOCIETY FOR CELL BIOLOGY
http://hdl.handle.net/10138/589795
Frisby, D, Murakonda, A B, Ashraf, B, Dhawan, K, Almeida-Souza, L, Naslavsky, N & Caplan, S 2024, 'Endosomal actin branching, fission, and receptor recycling require FCHSD2 recruitment by MICAL-L1', Molecular Biology of the Cell, vol. 35, no. 11, ar144. https://doi.org/10.1091/mbc.E24-07-0324

Endosomal actin branching, fission, and receptor recycling require FCHSD2 recruitment by MICAL-L1

Devin Frisby[a], Ajay B. Murakonda[a], Bazella Ashraf[a], Kanika Dhawan[a,b], Leonardo Almeida-Souza[c,d,e], Naava Naslavsky[a], and Steve Caplan[a,a,f,*]

[a]Department of Biochemistry and Molecular Biology, University of Nebraska Medical Center, Omaha, NE 68198; [b]Department of Pharmacology, School of Medicine, University of California, San Diego, La Jolla 92093, CA; [c]Helsinki Institute of Life Science, University of Helsinki, Helsinki 00790, Finland; [d]Institute of Biotechnology, University of Helsinki, Helsinki 00790, Finland; [e]Faculty of Biological and Environmental Sciences, University of Helsinki, Helsinki 00790, Finland; [f]Fred and Pamela Buffett Cancer Center, University of Nebraska Medical Center, Omaha, NE 68198

ABSTRACT **Endosome fission is required for the release of carrier vesicles and the recycling of receptors to the plasma membrane. Early events in endosome budding and fission rely on actin branching to constrict the endosomal membrane, ultimately leading to nucleotide hydrolysis and enzymatic fission. However, our current understanding of this process is limited, particularly regarding the coordination between the early and late steps of endosomal fission. Here we have identified a novel interaction between the endosomal scaffolding protein, MICAL-L1, and the human homologue of the *Drosophila* Nervous Wreck (Nwk) protein, FCH and double SH3 domains protein 2 (FCHSD2). We demonstrate that MICAL-L1 recruits FCHSD2 to the endosomal membrane, where it is required for ARP2/3-mediated generation of branched actin, endosome fission and receptor recycling to the plasma membrane. Because MICAL-L1 first recruits FCHSD2 to the endosomal membrane, and is subsequently responsible for recruitment of the ATPase and fission protein EHD1 to endosomes, our findings support a model in which MICAL-L1 orchestrates endosomal fission by connecting between the early actin-driven and subsequent nucleotide hydrolysis steps of the process.**

SIGNIFICANCE STATEMENT

- Endosome fission is crucial for receptor recycling and the ability of cells to transduce signals into the cell via surface expressed receptors. However, the mechanisms and proteins that regulate endosome fission are not fully understood.
- A new role for FCHSD2 is demonstrated in helping generate branched actin at endosomes and in promoting endosome fission. The authors demonstrate that the endosome scaffold, MICAL-L1, recruits FCHSD2 to endosomes via one of its two SH3 domains.
- Overall, these findings shed new light on the process of endosome fission, opening new avenues for further research in the field.

Monitoring Editor
Avital Rodal
Brandeis University

Received: Jul 29, 2024
Revised: Sep 25, 2024
Accepted: Oct 4, 2024

INTRODUCTION

The trafficking of internalized cargos through endocytic compartments and their recycling to the plasma membrane (PM) is critical to cellular function and necessary for plasma membrane homeostasis and the regulation of cell signaling pathways (Naslavsky and Caplan, 2018). Indeed, higher-order processes that are regulated by membrane trafficking include membrane remodeling, signal transduction, cell migration, and control of cell polarity (Wang *et al.*, 2000; Caswell and Norman, 2008; Cullen and Steinberg, 2018). Internalization at the plasma membrane occurs through various mechanisms of endocytosis, ultimately leading to the homotypic and heterotypic fusion of endocytic vesicles to generate the early or sorting endosome (EE/SE). At the EE/SE, cargos are actively sorted and shunted to different fates such as lysosomal degradation, retrograde trafficking to the Golgi, or recycling to the cell surface. Cargos destined for recycling are sorted and packaged into tubulovesicular structures that undergo fission and are either trafficked directly back to the plasma membrane (fast recycling) or first transported to the "endocytic recycling compartment," a series of perinuclear tubular recycling endosomes, before moving to the plasma membrane (slow recycling) (Xie *et al.*, 2016; Naslavsky and Caplan, 2018). While cargo recycling has previously been characterized as a passive or "default" process, recent studies support the notion that recycling is an active process mediated by cargo tail sorting signals and protein complexes that control recycling (Hsu *et al.*, 2012; McNally and Cullen, 2018). For example, ACAP1 mediates the sorting and recycling of various receptors, including the transferrin receptor (TfR), Glut4, and β1-integrin (Dai *et al.*, 2004; Li *et al.*, 2005; Bai *et al.*, 2012). Additionally, the retromer and retriever complexes cooperate with sorting nexins (SNXs) to regulate receptor sorting and recycling (Burd and Cullen, 2014; McNally *et al.*, 2017; Cullen and Steinberg, 2018; Wang *et al.*, 2018).

Both the retromer and retriever recycling complexes interact either directly or indirectly with the WASP and SCAR homologue (WASH) complex to activate ARP2/3-mediated branched actin polymerization (Gomez and Billadeau, 2009; Harbour *et al.*, 2012; Jia *et al.*, 2012; McNally *et al.*, 2017). The WASH complex is recruited to endosomes via direct interaction with the retromer complex, while the retriever complex is indirectly recruited to endosomes by the WASH complex through an interaction with the COMMD/CCDC22/CCDC93 (CCC) complex (Gomez and Billadeau, 2009; Jia *et al.*, 2012; Seaman *et al.*, 2013; McNally *et al.*, 2017). Interaction of the WASH complex with cargo recycling complexes highlights the role of actin in the early steps of cargo recycling at the endosome. Moreover, activation of ARP2/3-mediated branched actin polymerization establishes a physical barrier that helps form a cargo retrieval subdomain by inhibiting the diffusion of recycling receptors into the degradative endosomal subdomain (Puthenveedu *et al.*, 2010; Simonetti and Cullen, 2019). In addition, treatment of cells with branched actin inhibitors decreased recycling endosome tubulation, further establishing a crucial role for actin in the tubulation of cargo-laden vesicles on endosomes (Anitei and Hoflack, 2011; Delevoye *et al.*, 2016). During fission, actin provides a necessary pushing force at the neck of budding vesicles for constriction and generation of appropriate membrane tension (Derivery *et al.*, 2009; Gomez and Billadeau, 2009). Through its regulation of receptor sorting, endosome tubulation, and endosome fission, the WASH complex is required for T-cell receptor, GLUT1, β2AR, and a5β1-integrin recycling back to the plasma membrane; however, the proteins and mechanisms regulating actin polymerization and depolymerization at endosomes are largely unexplored (Temkin *et al.*, 2011; Zech *et al.*, 2011; Piotrowski *et al.*, 2013).

Coordination of fission at endosomes is complex and incompletely understood. It requires the function of multiple proteins in addition to the WASH complex, ARP2/3, and branched actin. Several models have been proposed for fission at endosomes (Solinger and Spang, 2022; Naslavsky and Caplan, 2023a; Gopaldass *et al.*, 2024). One recently elucidated mechanism for endosome fission is endoplasmic reticulum-driven fission, where branched actin patches containing Coronin1C stabilize cargo sequestration at tubular buds and recruit TMCC1 to drive fission (Rowland *et al.*, 2014; Hoyer *et al.*, 2018). However, it is unclear whether endoplasmic reticulum (ER)-based fission is primarily a mechanism for endosome homeostasis or whether it is key to vesicle/tubule carrier release and transport for recycling. Amphipathic helix insertion and the induction of positive membrane curvature is another mechanism that has been recently identified for endosome fission (Gopaldass *et al.*, 2017; Courtellemont *et al.*, 2022). Many models, however, favor a combination of initial actin-based membrane constriction followed by nucleotide hydrolysis of a dynamin-family fission protein to detach the budding vesicle/tubule ([Derivery *et al.*, 2009] and reviewed in [Naslavsky and Caplan, 2018, 2023a]).

The mode by which the earlier actin-based steps of endosomal membrane constriction are linked to the terminal steps of fission remain poorly defined. One crucial endosomal membrane hub and scaffolding protein is MICAL-L1 (Figure 1A). MICAL-L1 appears to be a master regulator of endosome fission; it localizes to endosomes and recruits a variety of proteins involved in both the early and late steps of endosome fission, including Syndapin2/PACSIN2 and EHD1 (Sharma *et al.*, 2009; Giridharan *et al.*, 2013). Syndapins may link membrane trafficking to cortical actin cytoskeletal dynamics, as they interact with dynamin and N-WASP (Qualmann *et al.*, 1999). EHD1 has been implicated in the later stages of fission (Naslavsky and Caplan, 2011; Cai *et al.*, 2012; Cai *et al.*, 2013; Cai *et al.*, 2014; Deo *et al.*, 2018; Kamerkar *et al.*, 2019; Dhawan *et al.*, 2020). Indeed, depletion of either MICAL-L1 or EHD1 leads to impaired fission and recycling (Naslavsky and Caplan, 2011; Cai *et al.*, 2012; Cai *et al.*, 2013; Cai *et al.*, 2014; Deo *et al.*, 2018; Kamerkar *et al.*, 2019; Dhawan *et al.*, 2020; Farmer *et al.*, 2021), and evidence suggests that EHD1 ATP hydrolysis drives its oligomerization on the endosomal membrane to induce membrane thinning and fission (Sharma *et al.*, 2009; Deo *et al.*, 2018). How MICAL-L1 coordinates the actin polymerization and membrane tubulation at endosomes that occurs during the early stages of cargo sorting with the later stages of EHD1-mediated endosome fission remains unknown.

This article was published online ahead of print in MBoC in Press (http://www.molbiolcell.org/cgi/doi/10.1091/mbc.E24-07-0324) on October 9, 2024.

Author contributions: D.F., B.A., K.D., and N.N. conceived and designed the experiments; D.F., A.B.M., B.A., K.D., and N.N. performed the experiments; D.F., A.B.M., B.A., K.D., and N.N. analyzed the data; D.F. drafted the article; D.F. prepared the digital images.

Conflicts of interest: The authors declare no financial conflict of interest.

*Address correspondence to: Steve Caplan (scaplan@unmc.edu).

Abbreviations used: CCC, COMMD/CCDC22/CCDC93; CME, clathrin mediated endocytosis; EGFR, epidermal growth factor receptor; ER, endoplasmic reticulum; FCHSD2, FCH and double SH3 domains protein 2; HRP, horseradish peroxidase; ITSN-1, intersectin-1; MHC-I, major histocompatibility class I; NMJ, neuromuscular junction; Nwk, Nervous Wreck; PM, plasma membrane; RPE-1, retinal pigmented epithelial-1; SH3, SRC homology 3; TCR, T cell receptor; TfR, transferrin receptor; WASH, WASP and SCAR homolog

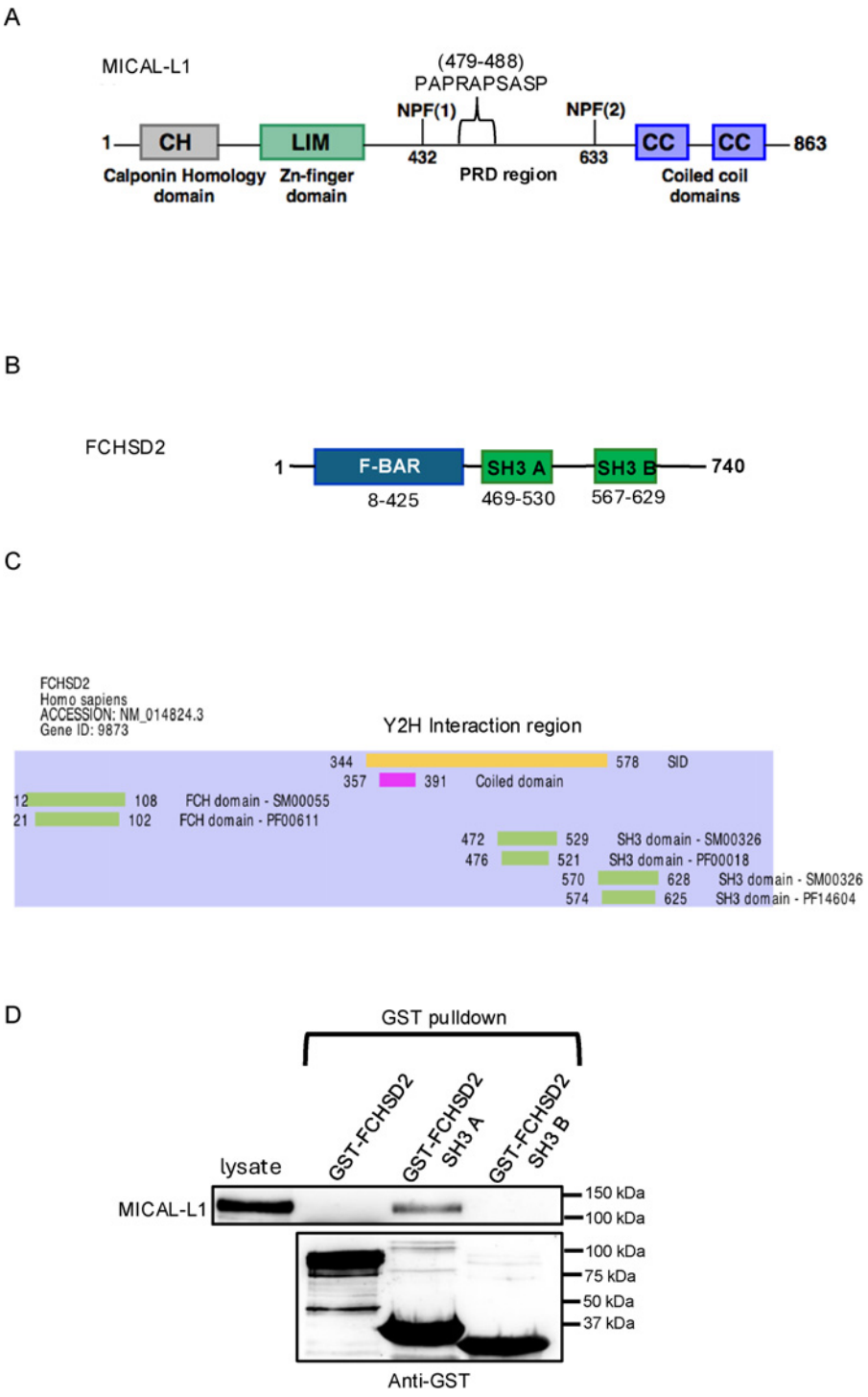

FIGURE 1: FCHSD2 interacts with MICAL-L1 via its first SH3 domain. (A) Domain architecture of MICAL-L1. (B) Domain architecture of FCHSD2. (C) An unbiased yeast 2-hybrid screen identified FCHSD2 as a MICAL-L1 interactor. MICAL-L1 was used as bait and an area covered by FCHSD2 amino acids 344-578 (yellow region, encompassing the first SH3 domain) was identified in the interaction. (D) GST pulldowns identified FCHSD2 SH3 A as the MICAL-L1 interacting domain. GST-FCHSD2, GST-FCHSD2 SH3 A, and GST-FCHSD2 SH3 B proteins were expressed in bacteria and purified. Purified protein (20 µg) was incubated with HeLa lysate and pulled down with Glutathione Sepharose resin. Samples were eluted, subjected to SDS–PAGE and immunoblotted with anti-GST and anti-MICAL-L1 primary antibodies. 20% of the overall volume used for the pulldown was run in the lysate sample. MICAL-L1 = Microtubule-associated monooxygenase, calponin and Lim domain containing-like1, FCHSD2 = FCH and double SH3 domains 2, CH = calponin homology, LIM = Lin11, Islet-1, and Mec-3, CC = coiled coil, BAR = Bin-Amphiphysin-Rvs, SH3 = Src homology 3, Y2H = yeast 2-hybrid, GST = glutathione S-Transferase.

Hit (protein name)	Confidence of Y2H	Priority for study	Reason
FCHSD2	Moderate	High	Has two SH3 domains that might interact with MICAL-L1 proline-rich domains, is involved in actin regulation, endocytic function. Implicated in fission at the plasma membrane.
CIN85 (SH3KBP1)	High	High	Under study. Has two SH3 domains that might interact with MICAL-L1 proline-rich domains, is involved in actin regulation, endocytic function.
CD2AP	Good	High	Under study. Has two SH3 domains that might interact with MICAL-L1 proline-rich domains, is involved in actin regulation, endocytic function. Homologous to CIN85
WDFY3 (ALFY)	Moderate	Moderate	FYVE domain containing protein localized to endosomes and involved in autophagy. Under study.
Syndapin3/PACSIN3	Moderate	Low	Involved in endosomal trafficking and actin regulation, but its paralogue Syndapin2/PACSIN2 has already been established as an interaction partner.
FBLN1 (Fibulin1)	Good	Low	Secreted glycoprotein, mostly extracellular. Unlikely partner for MICAL-L1.
FBN1 (Fibrillin1)	High	Low	Extracellular matrix glycoprotein with transmembrane domain and only 5 intracellular cytoplasmic residues. Unlikely partner for MICAL-L1.
Notch1	High	Low	Transmembrane receptor with significant intracellular regions, but Y2H binding predicted for extracellular region. Unlikely partner for MICAL-L1.

TABLE 1: Select yeast 2-hybrid hits using MICAL-L1 as bait.

To address this question, we took advantage of an unbiased yeast 2-hybrid screen and identified FCH and double SH3 domains protein 2 (FCHSD2) as a novel MICAL-L1 interacting partner. In this screen, we identified ~2 dozen potential interaction partners for MICAL-L1 and Table 1 includes eight of the top hits (see Table 1). Of note, Syndapin3/PACSIN3 was identified, a close paralogue of Syndapin2 which we have previously identified as a MICAL-L1 interaction partner (Giridharan *et al.*, 2013). Other proteins, although highly ranked in terms of potential for interaction, were deemed low priority based on their topology or other factors. Based on the domain architecture of FCHSD2, its known function thus far and its potential for involvement in endosome fission, we elected to prioritize the study of this interaction and its functional consequences.

FCHSD2 contains an N-terminal F-BAR domain, two SRC homology 3 (SH3) domains, and a C-terminal proline-rich region (Figure 1B). Initial insights into the function of FCHSD2 come from studies done in fruit flies with the *Drosophila* homologue, Nervous Wreck (Nwk). Adult temperature-sensitive Nwk mutants become paralyzed and experience spasms at 38°C (Coyle *et al.*, 2004). Investigations into the function of Nwk reveal that it regulates receptor signaling at neuromuscular junctions (NMJs) through its cooperation with the endocytic proteins Dap160 and WASP and the regulation of Cdc42/WASP-mediated branched actin polymerization (O'Connor-Giles *et al.*, 2008; Rodal *et al.*, 2008). FCHSD2 interacts with the corresponding mammalian homologues of Dap160 and WASP, intersectin-1 (ITSN-1) and N-WASP (Almeida-Souza *et al.*, 2018), respectively, as well as with dynamin (O'Connor-Giles *et al.*, 2008; Rodal *et al.*, 2008) and SNX9/18 (Haberg *et al.*, 2008), and FCHSD2 knockdown impedes cargo internalization via clathrin-mediated endocytosis (CME) (Almeida-Souza *et al.*, 2018; Xiao *et al.*, 2018). Indeed, FCHSD2 regulates CME by enhancing N-WASP/ARP2/3-mediated branched actin polymerization to promote maturation of clathrin-coated pits and facilitate dynamin-mediated fission and internalization (Almeida-Souza *et al.*, 2018). More recently, Nwk and FCHSD2 have been implicated in the regulation of cargo recycling at endosomes. Nwk localizes to Rab11-containing endosomes in *Drosophila* NMJs and regulates receptor trafficking through direct interaction with sorting nexin 16 (Rodal *et al.*, 2008; Rodal *et al.*, 2011), and Nwk mutants phenocopy RAB11 mutants for extracellular vesicle cargo transport (Blanchette *et al.*, 2022). Interestingly, FCHSD2 knockdown interferes with transferrin (Tf) and epidermal growth factor receptor (EGFR) recycling and subsequently leads to increased localization of these cargos with LAMP1, a marker of the lysosomal membrane (Xiao and Schmid, 2020). However, the mechanism by which FCHSD2 regulates cargo recycling at endosomes remains unknown.

Here we identify FCHSD2 as a novel MICAL-L1 interacting partner. MICAL-L1 knockout impairs FCHSD2 localization to endosomes. Consistent with previous findings, FCHSD2 depletion had a minor but significant decrease on uptake of both clathrin-dependent and -independent cargo. Importantly, FCHSD2 knockdown impaired the recycling of cargos from both internalization pathways. We show that upon FCHSD2 depletion, the size of EEA1-decorated and MICAL-L1–decorated endosomes increases, and we demonstrate that FCHSD2 knockdown significantly impedes endosomal fission. Moreover, FCHSD2 depletion decreases the concentration of branched actin at endosomes, supporting its function in activating branched actin polymerization and fission at endosomes.

RESULTS

MICAL-L1 interacts with and recruits FCHSD2 to endosomes

The execution of fission at the endosome is a complex process that requires tightly coordinated orchestration of multiple proteins in a sequential manner. MICAL-L1 (Figure 1A) is a key scaffold that, as described above, interacts with multiple endosomal proteins. However, a central question is how this scaffold coordinates the fission process and how it links nucleotide hydrolysis-driven fission with the earlier steps of membrane budding and constriction.

To identify novel MICAL-L1 interaction partners that might play a role in endosome fission, we used an unbiased yeast 2-hybrid approach to screen over 100,000,000 potential interactions with full-length MICAL-L1 as bait (Figure 1A). Among the potential hits identified with moderate confidence was the human homologue of the *Drosophila melanogaster* Nwk protein (Coyle *et al.*, 2004; Rodal *et al.*, 2008; Rodal *et al.*, 2011; Becalska *et al.*, 2013), known as FCH and double SH3 domains 2 (FCHSD2; also known as CAROM) (Ohno *et al.*, 2003; Xu *et al.*, 2017; Almeida-Souza *et al.*, 2018) (Figure 1B). Although primarily known for its role in internalization at the plasma membrane (Almeida-Souza *et al.*, 2018; Xiao and Schmid, 2020), recent studies have implicated mammalian FCHSD2 in receptor recycling (Xiao *et al.*, 2018; Xiao and Schmid, 2020). FCHSD2 has an F-BAR domain as well as two SH3 domains. Indeed, the binding region identified through the yeast 2-hybrid screen included the first of the two FCHSD2 SH3 domains, but not the second SH3 domain (Figure 1C). To validate this interaction, we generated and purified GST fusion proteins for full-length human FCHSD2 (GST-FCHSD2) and GST fused to either the first or second SH3 domain (GST-SH3 A and GST-SH3 B). Upon incubation with HeLa cell lysates, we demonstrated that whereas GST-FCHSD2 and GST-SH3 B were unable to pull down MICAL-L1, the isolated GST-SH3 A domain precipitated MICAL-L1 (Figure 1D). These data are consistent with a role for SH3 A in binding to MICAL-L1, likely via one or more of the latter's proline-rich motifs. The lack of binding for GST-FCHSD2 supports the notion that the full-length protein is in an autoinhibited conformation (Rodal *et al.*, 2008; Stanishneva-Konovalova *et al.*, 2016; Almeida-Souza *et al.*, 2018; Del Signore *et al.*, 2021).

The localization of FCHSD2 in mammalian cells has been studied primarily using exogenous protein, with reports indicating subcellular localization underneath the plasma membrane (Almeida-Souza *et al.*, 2018) and at actin protrusions (Zhai *et al.*, 2022b). Given the role of MICAL-L1 in scaffolding endosome fission machinery, we hypothesized that some FCHSD2 might be transiently localized to endosomes. To evaluate whether low concentrations of FCHSD2 are detectable on endosomes, we overexpressed GFP-FCHSD2 together with the active GTP-locked RAB5 mutant Q79L (Stenmark *et al.*, 1994). As expected, the RAB5 mutant induced and localized to enlarged endosomal structures (Figure 2A; inset in Figure 2B). Strikingly, FCHSD2 could be detected at the surface of these enlarged endosomes (Figure 2C; inset in 2D, and merged in Figure 2, E and F). To quantify the overlap between FCHSD2 and RAB5, we performed line scans on multiple images. We measured the relative intensity of the fluorescence for each channel along the line, normalizing the fluorescence by subtracting the "background" fluorescence from the cytoplasm. As demonstrated, the graph shows a peak of mean fluorescence for each channel, with the peak FCHSD2 (green) intensity overlapping with the peak RAB5 (red) intensity (Figure 2G). These data support the notion that FCHSD2 can be detected in proximity to RAB5 on the endosomal membrane.

Given that MICAL-L1 binds directly with lipids such as phosphatidic acid and phosphatidylserine (Giridharan *et al.*, 2013) and interacts with FCHSD2, we next hypothesized that MICAL-L1 is responsible for the initial recruitment of FCHSD2 to endosomes. To address this, we again used the RAB5 Q79L mutant to transfect either parental or MICAL-L1$^{-/-}$ HeLa cells (CRISPR/Cas9 knockout validated in Figure 2H). We first confirmed that endogenous FCHSD2 could be detected coating the membrane of enlarged RAB5 Q79L endosomes in the parental cells (Figure 2, I–K; quantified in Figure 2P). However, using an unbiased semiautomated quantification method (see Figure 2O for outline of segmentation method), significantly less FCHSD2 was observed on the RAB5 Q79L endosomes in the MICAL-L1$^{-/-}$ cells (Figure 2, L–N; quantified in Figure 2P). These data support the idea that MICAL-L1 is required for recruitment of FCHSD2 to the endosomal membrane.

FCHSD2 is required for internalization and recycling of clathrin-dependent and -independent cargo

Because MICAL-L1 has been implicated as an endosomal regulator that is required for receptor recycling and FCHSD2 can be detected on endosomes, we next tested whether FCHSD2 depletion impairs recycling of cargo from endosomes. We first assessed the impact of FCHSD2 depletion on TfR which is internalized through clathrin-mediated endocytosis. After 10 min of Tf uptake, FCHSD2-depleted cells (validated in Figure 3E) displayed a modest decrease in internalized TfR of ∼10%, consistent with previous studies (Almeida-Souza *et al.*, 2018; Xiao and Schmid, 2020) (Figure 3, A and C; quantified in Figure 3F). However, after a chase of 50 min to follow TfR recycling and the exit of labeled Tf from the cell, the FCHSD2 knockdown cells displayed a significant delay in endocytic recycling (normalized to levels of internalized TfR for each sample) (Figure 3, B and D; quantified in Figure 3G). These delays in recycling were consistent with those reported by Xiao and Schmid for both TfR and EGFR (Xiao and Schmid, 2020).

To determine whether FCHSD2 is involved in the recycling of receptors internalized through clathrin-independent means, we next analyzed the internalization and recycling of major histocompatibility complex class I (MHC I) receptors (Figure 4). Using both FCHSD2 siRNA knockdown and FCHSD2$^{-/-}$ cells (validated in Figure 4K), we demonstrated that whereas FCHSD2-depleted cells showed a modest decrease in internalized MHC I (Figure 4, A–D; quantified in Figure 4I), both FCHSD2 knockdown and knockout cells displayed delays in MHC I recycling, with the "acute" siRNA knockdown cells displaying more severe recycling defects than the "chronic" FCHSD2$^{-/-}$ cells (Figure 4, E–H; quantified in Figure 4J). Overall, our data support the notion that FCHSD2 plays an important role in regulating events at the endosome that are required for receptor recycling.

There is a growing appreciation that many endosomal proteins and endocytic regulatory proteins are also involved in regulating primary ciliogenesis (Madhivanan and Aguilar, 2014; Bales and Gross, 2016; Pedersen *et al.*, 2016). Moreover, because MICAL-L1 regulates ciliogenesis (Xie *et al.*, 2019; Xie *et al.*, 2023), we rationalized that its interaction partner FCHSD2 may also play a role in primary ciliogenesis. Accordingly, we asked whether FCHSD2 depletion impacts the ability of retinal pigmented epithelial cells (RPE-1) to generate a primary cilium. Upon FCHSD2 knockdown (validated in Supplemental Figure S1C), a greater percentage of serum-starved RPE-1 cells generated a primary cilium compared with mock-treated cells (Supplemental Figure S1, compare S1B with S1A; quantified in S1D). These data are consistent with a role for FCHSD2 in endocytic regulatory function and actin regulation, which has been linked to inhibition of ciliogenesis (Hoffman and Prekeris, 2022).

FCHSD2 is involved in the endosomal fission process

The fission of endosomes is required for formation of carrier vesicles/tubules and the recycling of receptors to the plasma membrane. Given the ascribed role for MICAL-L1 in endosome fission (Sharma *et al.*, 2009; Rahajeng *et al.*, 2012; Cai *et al.*, 2014; Farmer *et al.*, 2021), we postulated that FCHSD2 may regulate fission at

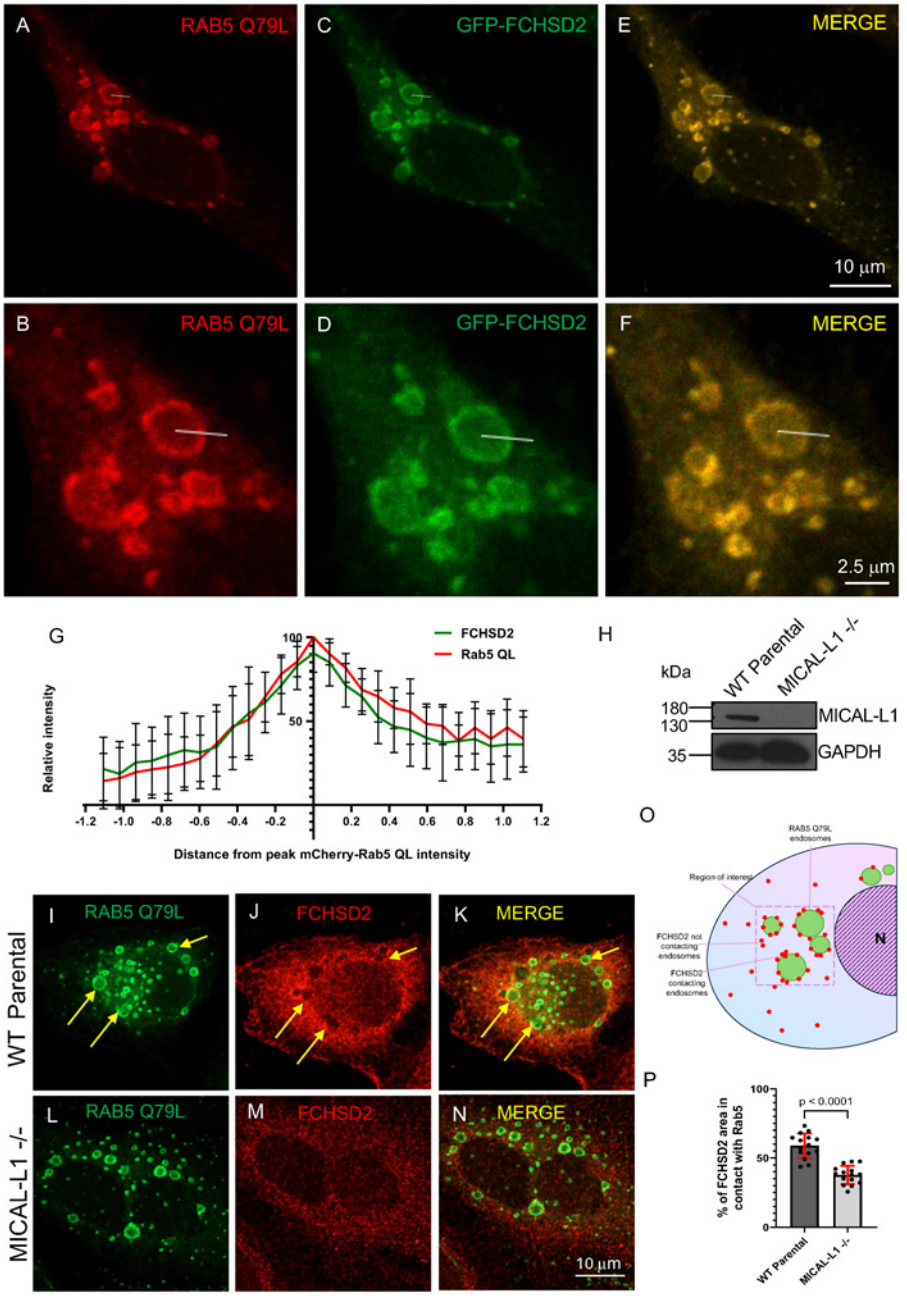

FIGURE 2: FCHSD2 is recruited to RAB5 QL endosomes by MICAL-L1. (A–F) HeLa cells were cotransfected with GFP-FCHSD2 and the mCherry-RAB5 Q79L mutant, which remains GTP-locked and active. Cells were fixed, imaged, and analyzed in ImageJ. B, D, and F represent insets of A, C, and E, respectively. A profile 2.81 µm in length was drawn from the cytoplasm into the enlarged mCherry-RAB5 Q79L endosomes, and the fluorescence intensities of both channels were collected along the line. Background subtraction was performed and the fluorescence intensities along each profile were normalized. (G) The data (quantified from from A–F) were plotted as relative intensity over the distance from peak mCherry-Rab5 Q79L intensity (red) and demonstrates that FCHSD2 staining overlaps with RAB5 Q79L on the endosomal membrane. (H) Immunoblot validation of MICAL-L1 knockout in the CRISPR/Cas9 gene-edited knockout cell line. (I–N) HeLa WT parental or MICAL-L1 knockout cells were transfected with the GFP-RAB5 Q79L mutant. Cells on coverslips were fixed after transfection and immunostained with anti-FCHSD2 to visualize endogenous FCHSD2 (J, M). Confocal images were captured and analyzed with Imaris software. As demonstrated, endogenous FCHSD2 coats RAB5 Q79L endosomes in parental cells (I–K; yellow arrows) but is largely absent from the endosomes in MICAL-L1 knockout cells (L–N). (O) Segmentation strategy for quantification of the percentage of FCHSD2 in contact with RAB5 Q79L endosomes. Square ROIs were made to include the maximal endosomal area within the ROI. (P) Quantification of I-N. In a demarked ROI around the RAB5 Q79L endosomes, the volume of FCHSD2 puncta that made contact with GFP-RAB5 Q79L endosomes was represented as a percentage of the total FCHSD2 volume in that region.

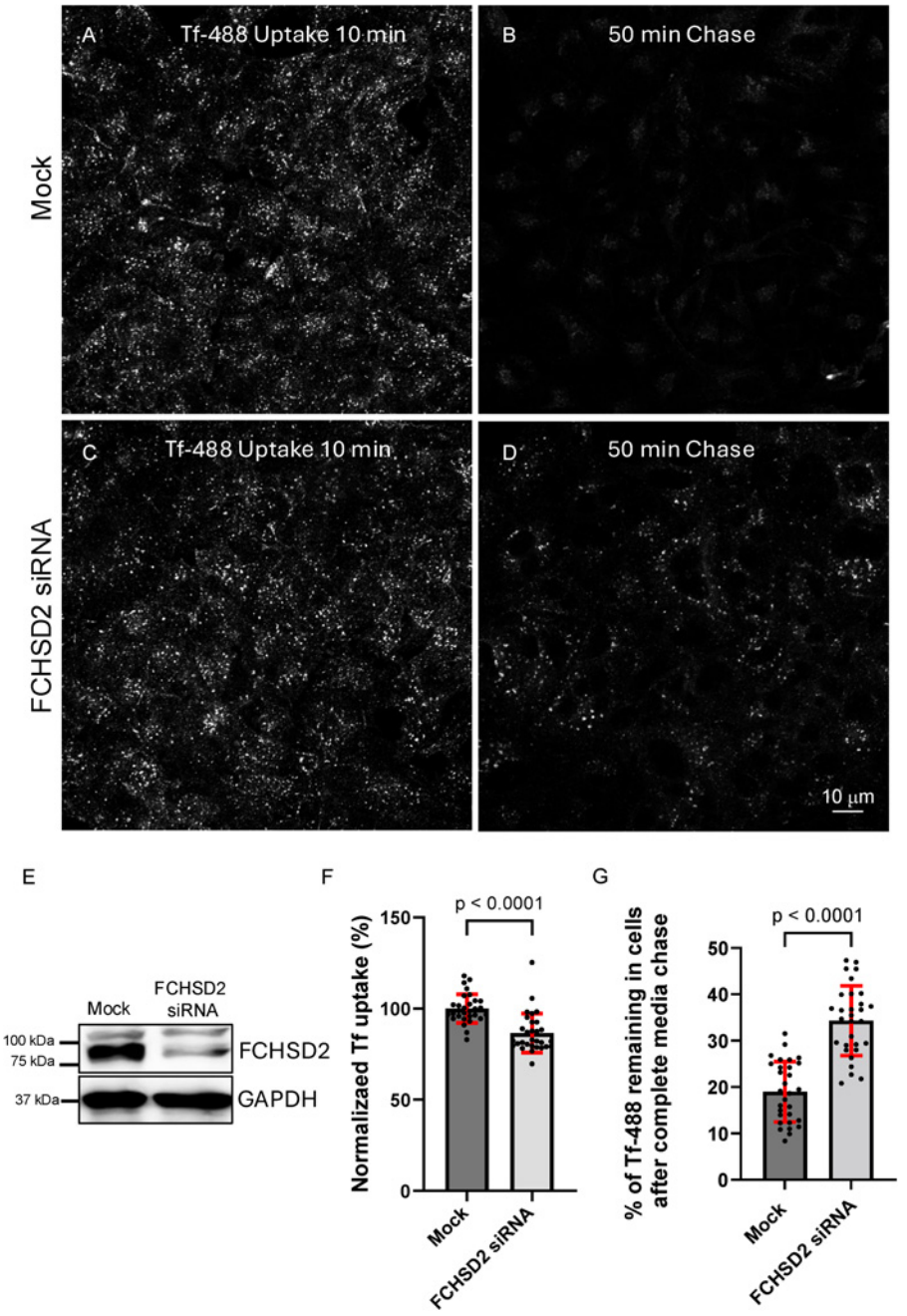

FIGURE 3: Tf uptake and recycling are impaired upon FHCSD2 depletion. (A–D) Mock and FCHSD2 siRNA knockdown HeLa cells on separate cover-slips were incubated with fluorophore-labeled transferrin (Tf-488) for 10 min (A, C) and chased with complete media for 50 min to allow recycling (B, D). Each image represents a distinct cover-slip/sample, fixed at the appropriate timepoint. (E) Immunoblot validation of FCHSD2 siRNA knockdown. (F) FCHSD2 depletion impairs Tf uptake. Images (similar to those in A and C) were analyzed in Zeiss Zen Blue software by measuring the arithmetic mean intensity of each image after uptake. For each of the three experiments, the mock internalized mean for all 10 samples was set at 100%, and each individual sample was plotted relative to this normalization. (G) FCHSD2 depletion delays Tf recycling. Images (similar to those in B and D) were analyzed in Zeiss Zen Blue software by measuring the arithmetic mean intensity of each image after recycling. Each "recycling" data point from the three independent experiments was compared with the normalized mean for uptake for that condition, which was set at 100%.

endosomes, potentially through its actin-regulatory activity. In recent years, it has become evident that in addition to punctate endosomes and endosomal carriers, many endosomes and endosomal carriers are tubular and their fission is regulated by MICAL-L1 and its interaction partners (Dhawan *et al.*, 2020; Jones *et al.*, 2020; Farmer *et al.*, 2021; Dhawan *et al.*, 2022). Accordingly, we asked whether the fission of punctate and tubular-shaped endosomes is impacted by depletion of FCHSD2 (Supplemental Figures S2 and S3). As shown, depletion of FCHSD2 by siRNA knockdown and in FCHSD2$^{-/-}$ cells (Supplemental Figure S2, B and D) led to

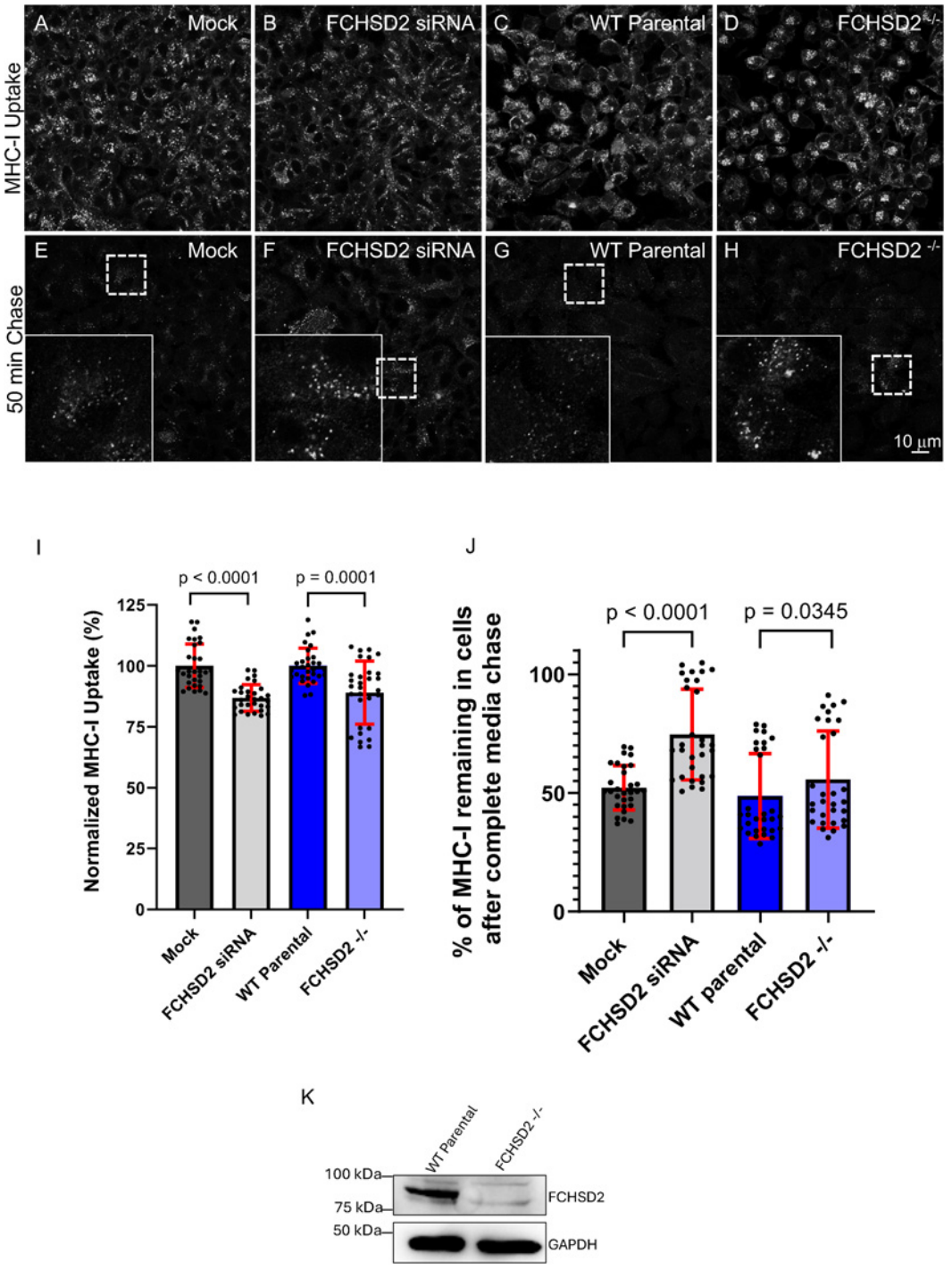

FIGURE 4: MHC-I uptake and recycling are impaired upon FCHSD2 depletion. (A–D) Mock, FCHSD2 siRNA knockdown, WT parental, and FCHSD2 knockout HeLa cells were incubated with anti-MHC-1 antibodies for 20 min (A–D). Cells were glycine stripped to remove noninternalized antibody, fixed, immunostained, and imaged. Each representative image is from a separate cover-slip fixed at the appropriate timepoint. (E–H) Following the 20 min uptake, cells were glycine stripped, washed, and chased with complete DMEM for 50 min to allow for MHC-I recycling. After chase, cells were glycine stripped again, fixed, and immunostained to detect nonrecycled MHC-I. Demarked regions are represented as insets. Each representative image is from a separate cover-slip fixed at the appropriate timepoint. (I) FCHSD2 depletion impairs MHC-I uptake. Images (including A–D) were analyzed in Zeiss Zen Blue software by measuring the arithmetic mean intensity of each image after uptake. For each of the three experiments, the mock internalized mean for all 10 samples was set at 100%, and each individual sample was plotted relative to this normalization. (J) FCHSD2 depletion impairs MHC-I recycling. Images (including E–H) were analyzed in Zeiss Zen Blue software by measuring the arithmetic mean intensity of each image after recycling. Each "recycling" data point from the three independent experiments was compared with the normalized mean for uptake for that condition, which was set at 100%. (K) Immunoblot validation of FCHSD2 CRISPR/Cas9 knockout in the CRISPR/Cas9 gene-edited knockout cell line (FCHSD2$^{-/-}$).

enlarged EEA1-marked endosomes (compare Supplemental Figure S2B with S2A and S2D with S2C; quantified in S2E). FCHSD2 knockdown also led to a longer and more elaborate tubular endosome network as compared with mock-treated cells (Supplemental Figure S3, compare S2B with S2A; quantified in Supplemental Figure S3H). Similarly, FCHSD2$^{-/-}$ cells also displayed an increase in total area of tubular endosomes marked by MICAL-L1 compared with the wild-type (WT) parental cells (Supplemental Figure S3, compare S3D with S3C; quantified in Supplemental Figure S3I). In addition, we transfected the FCHSD2$^{-/-}$ cells with WT FCHSD2. As shown, the FCHSD2-transfected cells (marked by red stars) displayed fewer tubular endosomes than untransfected cells (tubular MICAL-L1 endosomes marked by green arrows) (Supplemental Figure S3, E–G), and quantification showed a similar mean tubular endosome area to that observed in the WT parental cells (quantified in Supplemental Figure S3I). These data support the idea that FCHSD2 functions in the fission of EEA1 punctate endosomes and MICAL-L1–marked tubular endosomes.

While endosome size usually correlates negatively with fission in cells, size is also affected by fusion. To more definitively quantify the effects of FCHSD2 depletion on endosome fission, we took advantage of a novel in-cell fission assay that we recently developed that uses a synchronized system to acutely measure decrease in endosome size over a 30-min period (Dhawan *et al.*, 2022). Briefly, in mock and FCHSD2 knockdown cells, internalized Tf was used to mark endosomes, and both mock and knockdown cells were incubated with the PI3K inhibitor LY294002 to induce enlarged endosomes and allow synchronization of fission events upon inhibitor washout (chase). After inhibitor washout, in both mock-treated and FCHSD2-depleted cells, we imaged Tf-containing endosomes in three dimensions (3D) and quantified the mean size of more than 100,000 structures, measuring the frequency of structures from the binned endosome sizes (Figure 5, A–D; quantified in Figure 5, E–G). By integrating the area below each curve and subtracting the values from before and after the LY294002 washout (chase), we calculated and plotted a mean value for fission (Figure 5G). Additional experiments were done to measure the size of EEA1 endosomes (rather than Tf-containing endosomes), and they also demonstrated whereas mock-treated cells displayed reduced endosome size after LY294002 washout, FCHSD2 knockdown cells showed no significant reduction in size, suggesting impaired endosome fission (Supplemental Figure S4). Overall, these data strongly support a role for FCHSD2 in endosome fission.

FCHSD2 generates branched actin at the endosomal membrane

We next addressed the potential mechanism by which FCHSD2 regulates endosome fission. Given the role of FCHSD2 in actin regulation and control of WASP (Rodal *et al.*, 2008; Becalska *et al.*, 2013; Stanishneva-Konovalova *et al.*, 2016; Almeida-Souza *et al.*, 2018; Zhai *et al.*, 2022b), we hypothesized that FCHSD2 may regulate fission by activation of ARP2/3 leading to actin polymerization and branching at the endosomal membrane, thus facilitating membrane budding. Indeed, treatment of cells with the ARP2/3 inhibitor, CK-666 (Nolen *et al.*, 2009), led to significantly impaired actin filament generation at RAB5 Q79L enlarged endosomes, whereas the CK-689 control had no discernable effect on endosomal actin (Supplemental Figure S5, S5A–S5F; quantified in S5G and S5H), highlighting the role of ARP2/3 in generating branched actin at endosomes.

To determine whether FCHSD2 is required for ARP2/3-mediated endosomal branched actin, we used a modification of the elegant assay originally described by Cooper and colleagues (Zhao *et al.*, 2013) and applied on endosomes (Muriel *et al.*, 2016). Endogenous EEA1 was used as a marker of endosomes, and cortactin was used to identify branched actin in mock and FCHSD2 knockdown cells (Figure 6). We then segmented cells into "peripheral" and "perinuclear" regions. As demonstrated for the peripheral segmentations and quantification, mock-treated cells displayed a significantly higher percent of endosomes with branched actin marked by cortactin (Figure 6, C–E; see arrows in E-inset) than FCHSD2 knockdown cells (Figure 6, F–H and insets; quantified in Figure 6A). Contact between endosomes and cortactin in the perinuclear region (Figure 6B) was also modestly decreased, but given the high density of endosomes in that region, the periphery provides a better opportunity for quantification.

To better visualize actin and branched actin at endosomes in the presence and absence of FCHSD2, we transfected parental and FCHSD2 knockout cells with the GTP-locked RAB5 Q79L mutant, and then immunostained for branched actin (cortactin) (Figure 7). In parental cells, RAB5 Q79L induced formation of enlarged endosomes that were positive for cortactin and branched actin, often observed in a polarized manner at one or more region of the endosomal membrane (Figure 7, A–C, see arrows; quantified in Figure 7P). Strikingly, in FCHSD2 knockout cells branched actin and actin filaments were largely absent from the enlarged endosomes (Figure 7, D–F; quantified in Figure 7P). However, when FCHSD2$^{-/-}$ cells were rescued by transfection of WT FCHSD2 (see inset in Figure 7I displaying FCHSD2 transfection), the levels of cortactin observed on the enlarged endosomes increased and were more similar to those in the parental cells than the FCHSD2$^{-/-}$ cells (Figure 7, G–I; quantified in Figure 7P). Transfection with a FCHSD2 Y478A/Y480A SH3 A mutant (see inset in Figure 7L), that has impaired binding to proline-rich motifs (Almeida-Souza *et al.*, 2018) largely failed to rescue cortactin localization to endosomes (Figure 7, J–L; quantified in Figure 7P). However, transfection with FCHSD2 Y576S+F607S, an SH3 B interface mutant that fails to interact with intersectin 1 (Almeida-Souza *et al.*, 2018), nonetheless displayed significant rescue of branched actin generation at endosomes (despite its partial nuclear localization which may result from some degradation of the fusion protein), similar to that observed upon rescue with the WT FCHSD2 (Figure 7, M–O and see inset in Figure 7O; quantified in Figure 7P). MICAL-L1$^{-/-}$ cells were similarly devoid of branched actin (Supplemental Figure S6). The reconstitution of function in the FCHSD2$^{-/-}$ cells by the WT and SH3 B mutant did not reach 100% (~ 80–85%). Multiple possibilities might explain this, most notably the variance in expression levels of the reintroduced FCHSD2 proteins in individual cells that are assayed. Nevertheless, these data support the notion that MICAL-L1 recruits FCHSD2 by binding to its SH3 A domain to play a role in receptor recycling by activation of ARP2/3, a process which is required for the budding and fission of endosomes.

DISCUSSION

Many of the defined steps of CCP scission are analogous to fission at EE/SE, with the actin cytoskeleton playing a central role in the events at both membranes, and both processes will be referred to herein as "fission." Indeed, actin polymerization increases at clathrin-coated pits at the late stages of CCP internalization (Merrifield *et al.*, 2002), in concert with increased dynamin concentrations (Grassart *et al.*, 2014). At EE/SE, there is a dynamic polarized branched actin network that generates a pushing force on the endosome (Derivery *et al.*, 2009). Both CCP fission at the PM

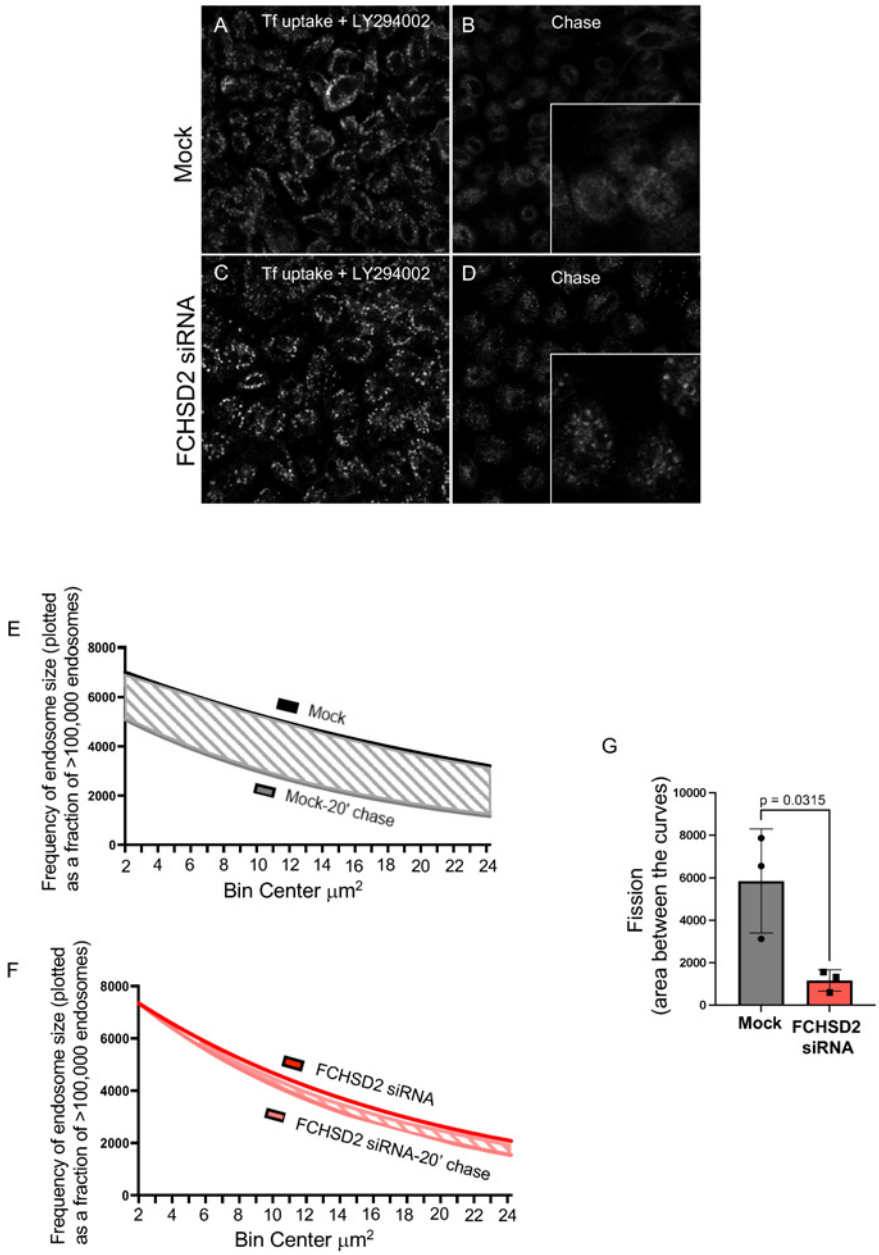

FIGURE 5: FCHSD2 depletion leads to impaired endosome fission. (A–D) Cells on coverslips were treated with the PI3K inhibitor LY294002 for 45 min to induce enlarged endosomes and synchronize the size of the endosome population. The cells were then incubated with Tf-488 in the presence of the inhibitor for 15 additional minutes. Cells were immediately fixed (uptake; A, C) or chased with complete media to washout the inhibitor and allow fission and recycling for 20 min (chase; B, D). (E–F) Imaris software was used to quantify and bin hundreds of thousands of endosomes according to mean size. The surface function in Imaris was used to render all of the Tf-containing structures. The surface areas of over 100,000 Tf-containing vesicles were plotted as a frequency distribution plot in GraphPad Prism. A frequency distribution (interleaved) graph with bins from 2 μm up to 10 μm and the bin width set at 1 μm was plotted, and a Gaussian curve was extrapolated beyond 10 μm to infinity on the frequency distribution graphs for all four experimental groups. (G) The area between the curves was calculated in GraphPad Prism by taking the difference between the area underneath the curves for uptake and chase in both experimental groups (E and F). The area between the curves represents a difference in the size of the endosomes after complete media chase, suggesting decreased fission in the FCHSD2 siRNA knockdown cells.

and endosome fission are facilitated by the ARP2/3 complex, which nucleates actin and generates branched actin (Pollard, 2007). However, the complex that serves as a nucleation promotion factor at endosomes and activates ARP2/3 is the WASH complex, whereas the N-WASP complex promotes branched actin via ARP2/3 at the PM (Merrifield *et al.*, 2004; Derivery *et al.*, 2009). An additional distinction between CCP and endosome fission is that the final step of CCP release requires GTP hydrolysis of dynamin, whereas evidence supports involvement of either dynamin (Derivery *et al.*, 2009) and/or the dynamin-family ATPase EHD1 in fission at the

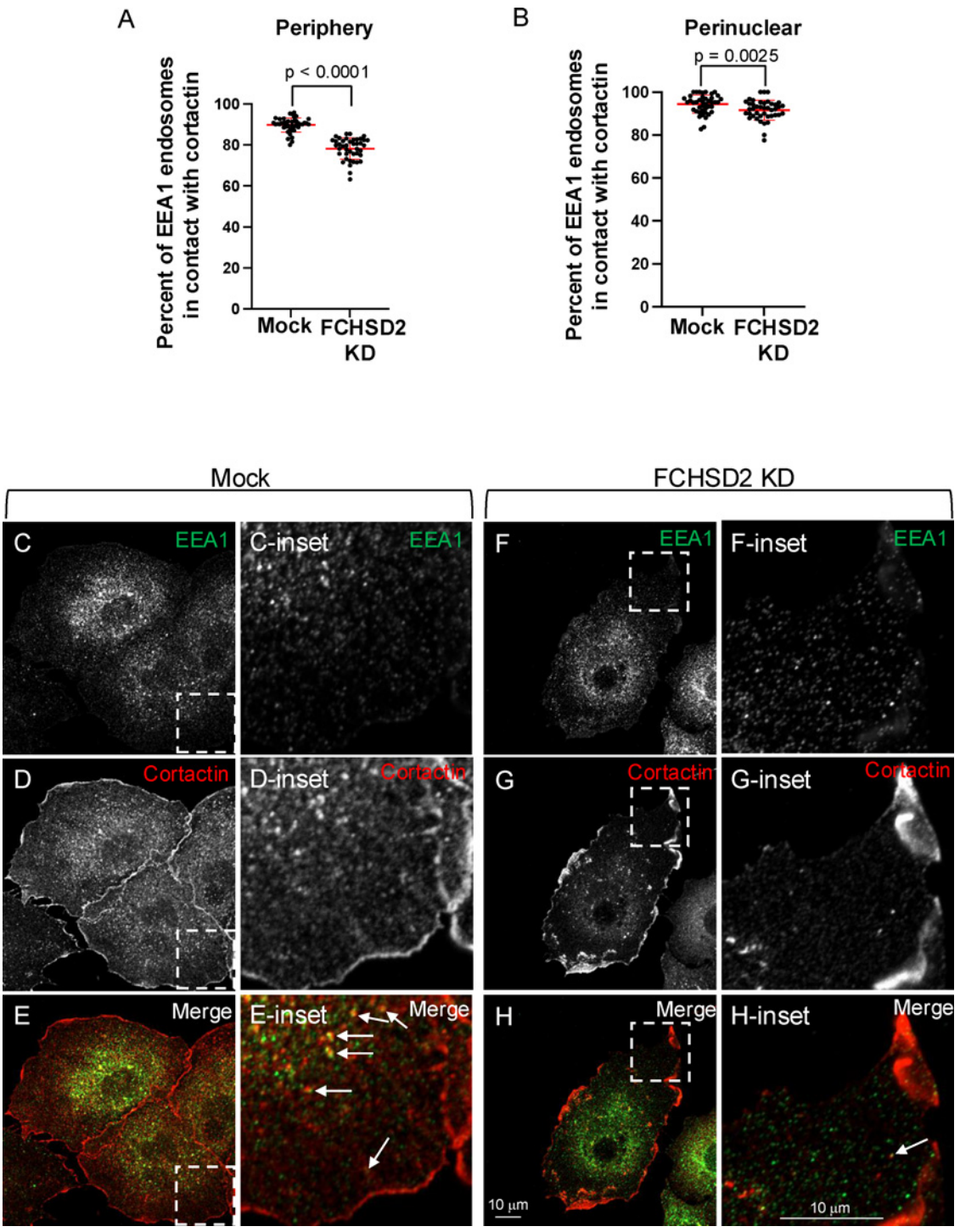

FIGURE 6: FCHSD2 knockdown leads to decreased branched actin at endosomes. (A, B) Quantification of C–H. Three ROIs were demarked in the periphery of the cells (ROI begins at a minimal distance of 5 µm from the nucleus), and another three regions in the perinuclear area (ROI begins within 1 µm from the nucleus). The surfaces function in Imaris was used to 3D render all of the EEA1 and cortactin structures. EEA1 structures contacting cortactin were defined as EEA1 surfaces with a shortest distance to a cortactin surface with a value equal to zero. The EEA1 structures that contacted cortactin were represented as a percentage of the total number of EEA1 structures in either the perinuclear region or the cell periphery. (C–E) Mock-treated NSCLC cells were fixed and immunostained with antibodies against cortactin (red) and EEA1 (green). Confocal images were captured and quantified (A, B). Insets of peripheral regions are shown. (F–H) FCHSD2 knockdown cells were fixed and immunostained with antibodies against cortactin (red) and EEA1 (green). Confocal images were captured and quantified (A, B). Insets of peripheral regions are shown. EEA1-decorated endosomes in mock-treated NSCLC cells contact cortactin puncta (white arrows) more frequently than the FCHSD2 knockdown cells.

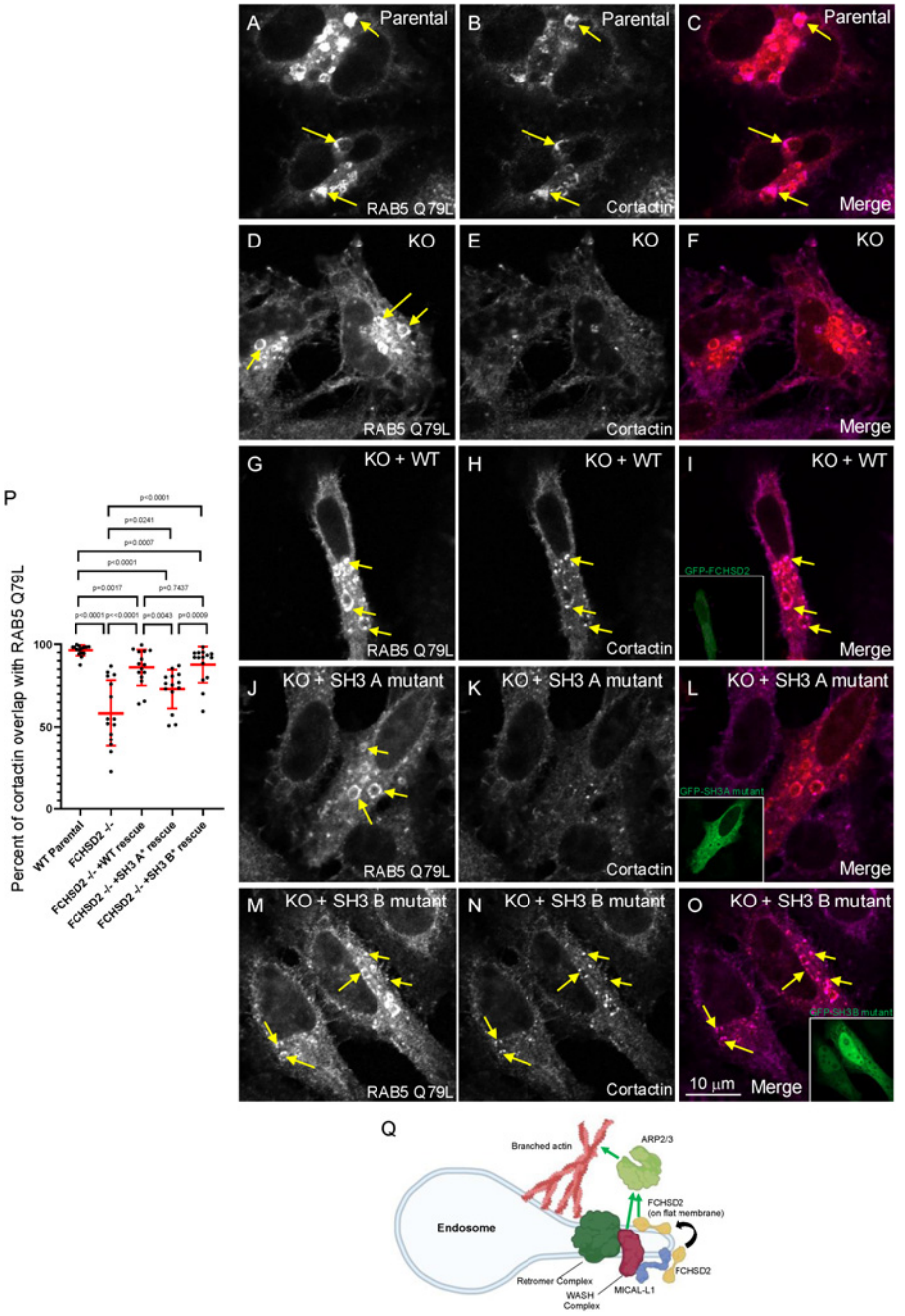

FIGURE 7: Visualization of decreased branched actin at endosomes in FCHSD2 knockdown cells. (A–O) WT parental (A–C), FCHSD2 knockout (D–F), FCHSD2 knockout + WT FCHSD2 rescue (G–I), FCHSD2 knockout + FCHSD2 SH3 A mutant rescue (J–L), and FCHSD2 knockout + FCHSD2 SH3 B mutant rescue (M–O) were transfected with mCherry-RAB5 Q79L. Cells were fixed and immunostained with an antibody against cortactin to mark branched actin. WT parental cells showed a robust cortactin localization at RAB5 Q79L endosomes (B, yellow arrows), whereas the FCHSD2 knockout cells show a significant decrease in cortactin localized to endosomes (E). Transfection of WT FCHSD2 rescued cortactin localization to the RAB5 endosomes (H, yellow arrows). Transfection with the FCHSD2 SH3 A mutant displayed impaired rescue of cortactin at endosomes (K), whereas transfection of FCHSD2 SH3 B mutant rescued cortactin endosomal localization (N, yellow arrows). These data suggest that the FCHSD2 SH3 A domain is required to promote branched actin polymerization at endosomes. (P) Quantification of A–O. Confocal Z-stack images were captured and analyzed by Imaris software using the surfaces function. mCherry-RAB5 Q79L structures were 3D rendered and a ROI around the enlarged endosomes was demarked. Cortactin puncta in this region were also 3D rendered. Cortactin surfaces that contacted RAB5 structures were filtered by setting the maximal "shortest distance to surface" at 1×10^{-7} nm. The volume of cortactin structures that contacted RAB5 structures was summed and represented as a percentage of the total cortactin volume in the designated ROI. (Q) Model for the role of FCHSD2 in fission at endosomes. FCHSD2 is recruited to and/or stabilized at endosomes through an interaction with MICAL-L1. FCHSD2 induces branched actin polymerization to promote endosome fission and receptor recycling. Insets in I, L and O indicate transfected cells.

endosome (Cai *et al.*, 2012; Cai *et al.*, 2013; Cai *et al.*, 2014; Deo *et al.*, 2018; Jones *et al.*, 2020; Kamerkar *et al.*, 2019). Finally, a key difference between CCP fission and endosomal fission is the involvement of different scaffold proteins in the process. At the PM, intersectin 1 plays an important role in the recruitment of the actin regulator FCHSD2 as well as dynamin (Sengar *et al.*, 1999; Almeida-Souza *et al.*, 2018), whereas at endosomes, we show that MICAL-L1 recruits FCHSD2 (Figures 1 and 2) and EHD1 (Sharma *et al.*, 2009). Notably, MICAL-L1 has been linked to microtubules (Xie *et al.*, 2019) and motor proteins (Rahajeng *et al.*, 2010), and the tension between microtubule-based pulling and branched actin pushing on membranes has been proposed as a unique feature in endosomes that causes membrane tension and leads to fission (Roux *et al.*, 2006).

MICAL-L1 is a RAB8 effector and key endosomal protein that localizes to both vesicular and tubular endosomes and recruits EHD1 to carry out the final steps of endosome fission (Sharma *et al.*, 2009; Sharma *et al.*, 2010; Giridharan *et al.*, 2012; Rahajeng *et al.*, 2012; Giridharan *et al.*, 2013; Cai *et al.*, 2014; Farmer *et al.*, 2021). In addition to its known role in recruiting players involved in the end stages of endosome fission, our new data now support a role for this scaffold in driving the early, actin constriction of endosomal membranes. Several lines of evidence suggest how MICAL-L1 may regulate the actin cytoskeleton at endosomes. First, MICAL-L1 interacts with Syndapin2/PACSIN2 (Giridharan *et al.*, 2013), a member of the Syndapin F-BAR containing proteins that constrict and tubulate membranes and regulate actin organization (Qualmann *et al.*, 1999; Qualmann and Kelly, 2000; Kessels and Qualmann, 2002; Dharmalingam *et al.*, 2009; Wang *et al.*, 2009). Second, recent studies provide evidence that MICAL-L1 interacts with two homologous proteins, CIN85 (also known as SH3-domain kinase binding protein 1) (Havrylov *et al.*, 2009; Huttlin *et al.*, 2017) and CD2AP (CD2-associated protein) (Huttlin *et al.*, 2021), each of which contains a capping protein interaction (CPI) motif that can interact with actin capping protein to promote actin branching (Cooper and Pollard, 1985; Bruck *et al.*, 2006; McConnell *et al.*, 2020). Notably, both these proteins come up as hits of good or high confidence, and current studies are underway to elicit their roles in endosome fission. Most significantly, we demonstrate here that MICAL-L1 interacts with the mammalian Nwk homologue, FCHSD2, which regulates actin assembly in flies and human cells (Rodal *et al.*, 2008; Stanishneva-Konovalova *et al.*, 2016; Almeida-Souza *et al.*, 2018; Del Signore *et al.*, 2021).

FCHSD2 has been implicated in receptor recycling (Xiao *et al.*, 2018; Xiao and Schmid, 2020) and Nwk localizes to recycling endosomes (Rodal *et al.*, 2011). Our findings, demonstrating that FCHSD2 regulates both the internalization and the recycling of clathrin-independent cargoes such as MHC-1, are consistent both with its interaction with MICAL-L1 and the latter's role in the regulation of tubular recycling endosomes and clathrin-independent cargo that selectively traverse this pathway (Sharma *et al.*, 2009; Sharma *et al.*, 2010; Rahajeng *et al.*, 2012; Giridharan *et al.*, 2013; Cai *et al.*, 2014; Xie *et al.*, 2016). Of interest, we observed that "acute" knockdown of FCHSD2 by siRNA typically had a more significant impact on fission and endocytic recycling than FCHSD2$^{-/-}$ knockout cells, except in the effect on MICAL-L1 tubular recycling endosomes where the impact was similar for both sets of experiments. On the one hand, the knockdown cells may display more significant phenotypes because unlike the CRISPR cells, FCHSD2 has not been depleted for long enough to facilitate compensation. On the other hand, the failure of the CRISPR knockout cells to undergo significant compensation with regard to MICAL-L1 tubular recycling endosomes highlights potential differences in the regulation of these pathways.

Consistent with roles for FCHSD2 in both endocytic function and actin regulation, FCHSD2 regulates ciliogenesis and knockout mice display acoustic vulnerability and hearing loss (Wang *et al.*, 2022; Zhai *et al.*, 2022a). Indeed, primary ciliogenesis is controlled both by endocytic events and by actin regulation (reviewed in Hoffman and Prekeris, 2022). Moreover, Nwk activates WASP to promote ARP2/3-dependent actin filament assembly (Stanishneva-Konovalova *et al.*, 2016), and similarly FCHSD2 stimulates ARP2/3 on flat membranes (Almeida-Souza *et al.*, 2018). FCHSD2 and CDC42 can also simultaneously bind N-WASP, providing an additional layer of actin regulation (Rodal *et al.*, 2008; Zhai *et al.*, 2022b). Given that the WASH complex is the major activator of endosomal ARP2/3 actin nucleation and WASH function is required for fission and receptor recycling (Derivery *et al.*, 2012; Derivery *et al.*, 2009), it is logical to speculate that FCHSD2 activates WASH at endosomes to promote ARP2/3-based actin nucleation. Our experiments do not distinguish whether the requirement for the FCHSD2 SH3 A domain in endosomal actin assembly is due to MICAL-L1 interactions, actin assembly through WASP family proteins, or both. However, we note that FCHSD2 is a dimer, and SH3A valency in vivo is likely even higher due to interactions with other binding partners. Therefore, FCHSD2 complexes on endosomes are likely capable of interacting with both MICAL-L1 and WASP family proteins. In addition, affinity capture-mass spectrometry has identified FCHSD2 as a SNX27 interactor (Shi *et al.*, 2021), a protein that binds directly to both the WASH complex and the retromer (Temkin *et al.*, 2011; Steinberg *et al.*, 2013), further supporting endosomal WASH complex activation. Indeed, our experiments show that FCHSD2 knockout cells have impaired branched actin generation at endosomes (Figure 7; Supplemental Figure S6), and that inhibition of ARP2/3 function leads to a failure to generate branched actin networks on endosomes (Supplemental Figure S5). Overall, these findings support a potential role for MICAL-L1 as a bridge or link between early actin-based steps of endosomal membrane constriction via FCHSD2 and EHD1-mediated fission of endosomes.

One intriguing question is what regulates the recruitment of FCHSD2 to endosomes? Nwk and FCHSD2 appear to be autoinhibited by both SH3 domains, although the SH3 B domain plays a more predominant role (Kelley *et al.*, 2015; Almeida-Souza *et al.*, 2018). It has been proposed that intersectin 1 recruits FCHSD2 to clathrin coats as they mature, by an atypical SH3-SH3 interaction with the SH3 B domain of FCHSD2, while keeping FCHSD2 in a state of low activation (Almeida-Souza *et al.*, 2018). Subsequently, PI(3,4)P2 accumulation at the edge of the CCP allows BAR domain binding and recruitment to the flat membrane surrounding the CCP. This in turn leads to the activation of FCHSD2 and induction of actin polymerization. At endosomes, however, MICAL-L1 recruitment of FCHSD2 is likely via one of the ~14 MICAL-L1 proline-rich domains with the SH3 A domain of FCHSD2 (Figure 1). We envision that analogous to the process at the PM, the BAR domain of FCHSD2 then interacts with endosomal phospholipids and is stabilized on the flat membrane region of endosomes to promote of branched actin generation. Indeed, FCHSD2 can bind to phosphatidylinositol(3,4,5)-trisphosphate (Almeida-Souza *et al.*, 2018) which is generated on endosomes by class I phosphatidylinositol-3-kinase activity (Jethwa *et al.*, 2015).

It is unclear at present whether FCHSD2 is "handed-off" from CCP at the PM to endosomes, or whether it is recruited from a cytoplasmic pool. However, recent studies have demonstrated that

stimulating receptor-mediated endocytosis leads to a significant increase in both the number and size of EE/SE (Naslavsky and Caplan, 2023b), as well as recruitment of EHD1 and fission machinery from the cytoplasm to endosomes (Dhawan *et al.*, 2020). As a result, this may lead to an increased level of MICAL-L1 available for the recruitment of FCHSD2. It is possible that FCHSD2 is recruited from CCP at the PM. In this scenario, the SH3-SH3 interactions between FCHSD2 and intersectin 1 may be higher affinity than the FCHSD2 SH3 A domain with MICAL-L1 proline-rich domains, but by increasing the availability of the MICAL-L1 binding sites for FCHSD2, increased recruitment of the latter protein may occur. Another possibility is that intersectin 1 itself is initially involved in FCHSD2 recruitment to endosomes. Indeed, a shortened form of intersectin (ITSN-s) serves as an effector for RAB13 (Ioannou *et al.*, 2017), ITSN-1 interacts with endosomal components such as RAB5 and ARF6 (Wong *et al.*, 2012), and ITSN-2 has been implicated in the regulation of endosomal recycling (Gubar *et al.*, 2020). However, the relationship between intersectins, MICAL-L1 and FCHSD2 at endosomes remains to be elucidated.

Our data are consistent with a model in which MICAL-L1 is initially required for recruitment of FCHSD2 to endosomal membranes (see model; Figure 7Q). This interaction occurs via the SH3 A domain of FCHSD2, and likely requires one of the multiple MICAL-L1 proline-rich domains domains. The identification of the specific proline-rich region(s) remains unknown, and it is possible that several such regions may be capable of binding. Once binding to MICAL-L1 occurs, we speculate that FCHSD2 migrates to extended regions of the budding endosomal membrane, consistent with its preference for flat membranes and select phosphoinositides (Almeida-Souza *et al.*, 2018). As a result, this membrane association helps stimulate WASH-mediated ARP2/3 activation of branched actin, leading to further membrane constriction and tubulation, supported by RAB and motor proteins (Farmer *et al.*, 2021). Ultimately, Coronin 1C (Hoyer *et al.*, 2018) and 2A (Dhawan *et al.*, 2022) have been implicated in clearance of branched actin, providing accessibility for the MICAL-L1 partner and fission protein, EHD1, to the membrane, leading to vesicle/tubule release and cargo recycling to the PM. Overall, our study provides new insight into the mechanisms of EE/SE fission, and helps identify how actin-based constriction events are coupled with nucleotide hydrolysis to promote fission.

MATERIALS AND METHODS

Request a protocol through *Bio-protocol*

Antibodies and reagents

The following antibodies were used: anti-MICAL-L1 (1794, LifeTein, 1:200 for immunoblotting), anti-GST-HRP (A01380, Genscript, 1:500), anti-GAPDH-HRP (HRP-60004, Proteintech, 1:5000), anti-FLAG (F1804, Sigma, 1:800), anti-FCHSD2 (described in Almeida-Souza *et al.*, 2018, 1:300 for immunostaining), anti-FCHSD2 (PA5-58432, Invitrogen, 1:250 for immunoblotting), anti-MHC-1 (purified W6/32, Leinco Technologies), anti-EEA1 (3288, Cell Signaling Technology, 1:30), anti-cortactin (05-180-I, Sigma, 1:200), anti-acetylated tubulin (3971, Cell Signaling Technology, 1:300), anti-CP110 (12780, Proteintech, 1:200), anti-MICAL-L1 (H00085377-B01P, Novus, 1:500 for immunostaining), anti-MICAL-L1 (ab220648, Abcam, 1:300 for immunostaining), donkey anti-mouse-HRP (715-035-151, Jackson, 1:5000), mouse anti-rabbit IgG light chain-HRP (211-032-171, Jackson, 1:3000), Alexa Fluor 568–conjugated goat anti-rabbit (A11036, Molecular Probes, 1:500), Alexa Fluor 568–conjugated goat anti-mouse (A21043, Molecular Probes, 1:500), Alexa Fluor 488–conjugated goat anti-rabbit (A11034, Molecular Probes, 1:500), Alexa Fluor 488–conjugated goat anti-mouse (A11029, Molecular Probes, 1:500), and Alexa Fluor 647–conjugated goat anti-mouse (115-606-008, Jackson ImmunoResearch, 1:750). The following plasmid constructs were used: GFP-RAB5 Q79L (Roberts *et al.*, 1999), mCherry-RAB5 Q79L (35138, Addgene), FLAG-FCHSD2 (GenScript), FCHSD2-GFP (Almeida-Souza *et al.*, 2018), FCHSD2 Y576S+F607S – GFP (Almeida-Souza *et al.*, 2018), and FCHSD2 YY478/480AA-GFP (Almeida-Souza *et al.*, 2018). The following reagents were used: Sepharose resin (L00206, GenScript), Alexa fluor 488–conjugated Tf (T13342, Invitrogen), CF-568–conjugated Phalloidin (44-T VWR, Biotium, 1:100), PI3K inhibitor LY294002 (501099125, Thermo Fisher Scientific), CK-689 (182517, MilliporeSigma), and CK-666 (182515, MilliporeSigma). Yeast 2-hybrid screens of over 100,000,000 potential interactions were performed by Hybrigenics (Boston, MA) using the full-length WT MICAL-L1 as bait.

Cell culture and treatments

The HeLa cell line (ATCC-CCL-2) was obtained from ATCC and cultured with complete DMEM (high glucose) (Thermo Fisher Scientific, Carlsbad, CA) with 10% FBS (Sigma-Aldrich), 1 × penicillin-streptomycin, and 2 mM L-glutamine. The hTERT RPE-1 human epithelial cell line (ATCC-CRL4000) was obtained from ATCC and grown in DMEM/F12 (Thermo Fisher Scientific, Carlsbad, CA) with 10% FBS, 1 × penicillin-streptomycin, 2 mM L-glutamine, and 1X non-essential amino acids (Thermo Fisher Scientific, Waltham, MA). The non–small cell lung cancer cell (NSCLC) line H-1650 was obtained from ATCC (CRL-5883) and cultured in RPMI with 10% FBS, 1 × penicillin-streptomycin, 2 mM L-glutamine, 1X MEM non-essential amino acids, 25 mM HEPES, and 1 mM sodium pyruvate. Validated CRISPR/Cas9 gene-edited HeLa knockout cells (FCHSD2$^{-/-}$ and MICAL-L1$^{-/-}$) were obtained from GenScript (Piscataway, NJ). All media also contained 100 µg/ml Normocin (Invitrogen) to prevent *Mycoplasma* and other contamination and cells were routinely tested for *Mycoplasma* contamination. All cells were cultured at 37°C in 5% CO_2. The small interfering siRNA (siRNA) oligonucleotide targeting human FCHSD2 (5′-GCAUACUCCUGAGACCUCA[dT][dT]-3′) was obtained from Sigma-Aldrich. FCHSD2 siRNA knocdown in all HeLa cell lines was performed for 48 h using the DharmaFECT transfection reagent (Dharmacon, Lafayette, CO). To achieve knockdown in both RPE and NSCLC cells, siRNA was transfected using the Lipofectamine RNAi/MAX (Invitrogen, Carlsbad, CA) reagent for 72 h. Knockdown efficiency was confirmed via immunoblotting. Transfection with FCHSD2 constructs and RAB5 Q79L constructs was achieved using the FuGENE 6 (Promega, Madison, WI) transfection reagents and protocol. The DNA ratios used for cotransfections are noted below.

Immunoblotting

Cultured cells were washed three times with ice-cold PBS and harvested with a cell scraper. Pelleted cells were resuspended in lysis buffer (50 mM Tris–HCl pH 7.4, 150 mM NaCl, 1% NP-40, 0.5% sodium deoxycholate) with freshly added protease inhibitor cocktail (Roche, Indianapolis, IN) for 30 min on ice. Lysates were then centrifuged at 13,000 rpm at 4°C for 10 min. Following centrifugation, 4x loading buffer was added to each sample and then boiled for 10 min. Collected lysates or samples from the GST pulldowns were separated by 10% SDS–PAGE, and transferred onto a nitrocellulose membrane (GE Healthcare, Chicago, IL). After membrane transfer, the membranes were blocked with 5% dried milk in PBS containing 0.3% (vol/vol) Tween-20 (PBST) for 30 min at room tem-

perature. The membrane was incubated with the primary antibody diluted in PBST at 4°C overnight. The membrane was washed three times with PBST after incubation with the primary antibody and then incubated at room temperature for 30 min with the appropriate horseradish peroxidase (HRP)-conjugated secondary antibody diluted in PBST. Enhanced chemiluminescence (Bio-Rad, Hercules, CA) was used to visualize the HRP-conjugated secondary antibody and digital images were acquired with iBright Imaging Systems (Invitrogen).

Recombinant gene expression and protein purification

The GST-tagged FCHSD2 DNA constructs were transformed into *Escherichia coli* Rosetta strain, and freshly transformed *E. coli* was inoculated in 50 ml of Luria-Bertani (LB) broth, containing 100 µg/ml ampicillin. Following an overnight incubation at 37°C with shaking, the 50 ml culture was used to inoculate a 1000 ml LB culture (containing antibiotic), which was incubated at 37°C with shaking until the optical density reached 0.4–0.6 at 600 nm. Protein expression was then induced with 1 mM IPTG, and the culture was incubated overnight at 18°C. The bacteria were then centrifuged at 5000 rpm for 15 min at 4°C. The bacterial pellet was then resuspended in ice-cold lysis buffer composed of 1x PBS (pH 7.4) and one tablet of protease inhibitor (Roche) per 10 ml. Following resuspension, the sample was lysed on ice via sonication (10 min of total sonication with 20 s on and 10 s off cycles). To separate the cellular debris, lysates were then centrifuged at 19,000 rpm for 45 min at 4°C. The supernatant was then incubated with Glutathione Sepharose resin overnight at 4°C. Three subsequent washes were performed with 10-bed volumes of wash buffer, which was composed of 1x PBS with protease inhibitor.

GST pulldown

Following protein purification, 20 µg of bead-bound GST constructs were centrifuged at 13,000 rpm for 30 s and resuspended in 30 µl of 1x PBS. 1 U micrococcal nuclease was added to the bead-bound protein and incubated at 30°C for 10 min. Following this incubation, HeLa cell lysate (lysed with 1% Brij98, 25 mM Tris-HCl, 125 mM NaCl, 1 mM $MgCl_2$, protease inhibitor, pH 7.4) was added to the bead-bound protein and incubated at 4°C for 3 h. The samples were then washed three times with 10-bed volumes of wash buffer (0.1% Brij98, 25 mM Tris-HCl, 125 mM NaCl, 1 mM $MgCl_2$, protease inhibitor, pH 7.4) and eluted with 4x loading buffer before undergoing SDS–PAGE and immunoblotting.

FCHSD2 localization at RAB5 endosomes

HeLa cells were plated on coverslips and cotransfected with GFP-FCHSD2 and mCherry-RAB5 Q79L (1:1) using the FuGene transfection system. Following overnight transfection, coverslips were fixed with 4% paraformaldehyde (in PBS) for 20 min at room temperature. After fixation, the coverslips were washed 3x with PBS and mounted in Fluoromount (Thermo Fisher Scientific). Confocal images were captured using a Zeiss LSM 800 confocal microscope (Carl Zeiss) with a 63 ×/1.4 NA oil objective, and the images were analyzed in ImageJ (National Institutes of Health, Bethesda, MD). In ImageJ, a profile 2.81 µM in length was drawn from the cytoplasm into the enlarged mCherry-RAB5 Q79L vesicles. The fluorescence intensities along the profile were collected for both the red and the green channels. Background subtraction was performed using the background fluorescence intensity in the region of the cytoplasm devoid of mCherry-RAB5 Q79L vesicles. Following background subtraction, fluorescent intensities along the profile were calculated as relative intensities of the maximal intensity for both the red and the green channels. The distance from the maximal mCherry-RAB5 Q79L fluorescent intensity was normalized for each figure and plotted. Localization of endogenous FCHSD2 at GFP-RAB5 Q79L structures in WT parental and MICAL-L1 knockout cells was quantified using Imaris 9.9.1 software. A region of interest (ROI) containing the RAB5 vesicles was marked, and all FCHSD2 puncta and RAB5 Q79L structures in that area were three-dimensionally (3D)-rendered (see parameters: Table 2, Rows 1 and 2). The volumetric sum of all FCHSD2 puncta that contacted a RAB5 Q79L structure was calculated as a percentage of the entire FCHSD2 volume in that ROI.

Recycling assays

The Tf recycling assay was performed by diluting Transferrin-Alexa Fluor 488 (Tf-488; Invitrogen) 1:700 in complete DMEM. FCHSD2 siRNA- or mock-treated cells were allowed to uptake TF for 10 min at 37°C. Following uptake, cells were washed twice with 1x PBS and then chased with complete DMEM for 50 min. After three washes with 1x PBS, cells were fixed with 4% paraformaldehyde in PBS for 20 min and then mounted in Fluoromount. For the MHC-1 recycling assay, cells were incubated with anti-MHC-1 antibody diluted in complete DMEM for 20 min at 37°C. After uptake, the remaining antibodies bound to the cell surface MHC-1 were removed via a 1-min glycine strip (0.1 M HCl-glycine, pH 2.7). The glycine-stripped cells were then either washed and fixed (uptake group) or washed three times with 1x PBS, chased with complete DMEM for 50 min at 37°C and restripped. The cells were then washed three times with PBS and fixed with 4% paraformaldehyde in PBS for 20 min. Cells were then stained with fluorochrome-conjugated secondary antibodies for 30 min, washed three times with PBS, and mounted in Fluoromount. Confocal images of cells after both the Tf and MHC-1 recycling assays were captured using a Zeiss LSM 800 confocal microscope (Carl Zeiss) with a 63 ×/1.4 NA oil objective. The arithmetic mean of fluorescence intensity for each image was analyzed using Zen Blue software. For uptake experiments, the mean of each mock-treated sample from the three independent experiments was normalized to 100%, and FCHSD2-siRNA transfected samples were compared with this. For calculating recycling, each data point from the three independent experiments was compared with the normalized mean measured for uptake for that condition, which was set at 100%.

Measurement of endosome size

FCHSD2 siRNA- or mock-treated HeLa cells were fixed with 4% paraformaldehyde (PBS) for 20 min at room temperature. After fixation, the cells were stained with anti-EEA1 for 1 h and the appropriate fluorochrome-conjugated secondary antibody for 30 min at room temperature. The coverslips were mounted, and images were captured using a Zeiss LSM 800 confocal microscope (Carl Zeiss) with a 63 ×/1.4 NA oil objective. EEA1 area was measured using Imaris 9.9.1 by rendering surfaces according to the settings listed on Table 2, Row 3. For measuring MICAL-L1 endosome area, FCHSD2 knockout cells were transfected with Flag-FCHSD2 as the rescue group. WT parental, FCHSD2 knockout, knockout + rescue, mock-treated, and FCHSD2 siRNA-treated cells were fixed (as described above) and stained with anti-MICAL-L1. The MICAL-L1 area per cell was measured using Imaris 9.9.1 with settings according to Table 2, Row 4.

Fission assay

Mock- and FCHSD2 siRNA-treated HeLa cells were incubated for 45 min in DMEM containing 80 µM of the PI3K inhibitor LY294002

Reference number	Description	Surface grain size (μm)	Diameter of largest sphere (μm)	Manual threshold value	Region growing estimated diameter (μm)	Quality above
1	FCHSD2 localization: FCHSD2 puncta	0.0800	0.200	740.43	0.600	−0.181
2	FCHSD2 localization: Rab5 QL structures	0.0500	0.400	5194.76	0.500	3962
3	Endosome morphology: EEA1	0.0500	0.400	4073.89	0.500	6679
4	Endosome morphology: MICAL-L1	0.198	1.00	5751.4	N/A	N/A
5	Fission assay: Tf and EEA1	0.250	3.48	5746	1.30	427
6	Cortactin at Rab5 QL: mCherry-Rab5 QL	0.0500	1.00	9696.54	0.500	5148
7	Cortactin at Rab5 QL: GFP-Rab5 QL	0.0500	0.400	5194.76	0.500	3962
8	Cortactin at Rab5 QL: Cortactin	0.0800	0.200	3388.84	0.600	−0.128
9	EEA1-Cortactin contacts: EEA1	0.200	0.638	2.69884	N/A	N/A
10	EEA1-Cortactin contacts: cortactin	0.170	0.543	2.46539	N/A	N/A

TABLE 2: Imaris parameters table.

(Cayman Chemical, Ann Arbor, MI) diluted for 1 h at 37°C. Following the initial incubation, cells were washed with PBS and then incubated in DMEM containing Transferrin-Alexa Fluor 488 (Invitrogen) and 80 μM LY294002 for 15 min at 37°C. Cells were then washed with PBS to remove the inhibitor and chased with complete DMEM for 20 min to allow synchronized fission and recycling. Finally, cells were washed three times with PBS and fixed with 4% paraformaldehyde in PBS for 20 min at room temperature. Cells on coverslips were incubated with anti-EEA1 for 1 h, followed by three PBS washes and a 30-min incubation with the appropriate 568 fluorochrome–conjugated secondary antibody. After staining, coverslips were mounted in Fluoromount, and images were captured using a Zeiss LSM 800 confocal microscope (Carl Zeiss) with a 63 ×/1.4 NA oil objective. Quantification of the assay was done using surface rendering in Imaris 9.9.1. Tf-containing vesicles and EEA1-decorated endosomes were 3D rendered according to the parameters on Table 2, Row 5. The size of Tf-containing vesicles was plotted in GraphPad Prism as a frequency distribution (interleaved) graph with bins from 2 μm to 10 μm and the bin width set at 1 μm. A Gaussian curve was plotted to infinity on the frequency distribution graphs for all four experimental groups (mock uptake, mock chase, knockdown uptake, knockdown chase). The area under each of the curves was calculated using the "Area under the curve" function in GraphPad Prism 10.2.3. The area between the curves for the mock- or siRNA-treated group was calculated as the area under the curve after uptake minus the area under the curve after chase.

Quantification of cortactin at RAB5 QL endosomes

Experimental groups included HeLa WT parental, FCHSD2 knockout cells, and FCHSD2 knockout cells transfected with FCHSD2-GFP, FCHSD2 YY478/480AA-GFP, or FCHSD2 Y576S+F607S-GFP. Cells were transfected with mCherry-RAB5 Q79L (Addgene #35138; 1:1 in cells with cotransfection) overnight. GFP-RAB5 Q79L was transfected into WT parental, FCHSD2 knockout, and MICAL-L1 knockout cells. Cells were washed with PBS and fixed with 4% paraformaldehyde in PBS for 20 min at room temperature. Following fixation, cells were stained with anti-cortactin for 1 h, followed by three washes with PBS and a 30-min incubation with the appropriate 647 fluorochrome–conjugated secondary antibody. Three additional washes with PBS were performed after secondary incubation, and then the cells were mounted in Fluoromount. Z-stacks were captured using a Zeiss LSM 800 confocal microscope (Carl Zeiss) with a 63 ×/1.4 NA oil objective. Using Imaris 9.9.1 software, mCherry-RAB5 Q79L and GFP-RAB5 Q79L structures were 3D-rendered (see Table 2, Rows 6 and 7, respectively). A ROI around the active Rab5 structures was demarked, and cortactin structures in this region were 3D-rendered (see Table 2, Row 8). The cortactin structures that contacted the active RAB5 structures were selected using the filter tab and setting the maximal "shortest distance to surface" at 1×10^{-7} nm. The volume of cortactin structures that contacted RAB5 structures was summed and represented as a percentage of the total cortactin volume in the designated ROI.

Actin inhibitors

HeLa cells were plated on coverslips and transfected with GFP-RAB5 Q79L. The following day, the cells were incubated for 40 min with 300 μM of either the control CK-689 or the specific ARP2/3 inhibitor CK-666 diluted in complete DMEM. Following the incubation, the cells were washed with PBS and fixed with 4% paraformaldehyde in PBS for 20 min. The cells were then washed three times with PBS and stained with 568-phalloidin for 1 h to mark the filamentous actin network. The cells were washed an additional three times and then mounted on slides in Fluoromount. Confocal images were captured using a Zeiss LSM 800 confocal microscope (Carl Zeiss) with a 63 ×/1.4 NA oil objective.

EEA1-Cortactin contacts

Mock- and FCHSD2 siRNA-treated NSCLC cells were washed with PBS and fixed with 4% paraformaldehyde in PBS for 20 min. The cells were costained with anti-EEA1 and anti-cortactin antibodies by incubating with the primary antibody at room temperature for 1 h. The cells were subsequently washed three times with PBS and incubated with the appropriate fluorochrome-conjugated secondary antibodies. Following another three washes with PBS, cells were mounted in Fluoromount, and images were captured using a Zeiss LSM 800 confocal microscope (Carl Zeiss) with a 63 ×/1.4 NA oil objective. Images were quantified in the Imaris 9.9.1 software using the surfaces function with the respective parameters for EEA1 (Table 2, Row 9) and cortactin (Table 2, Row 10). Three ROIs were demarked in the periphery of the cells (defined as an area with no border closer than 5 μm to the nucleus), and another three regions in the perinuclear area (defined as an area having a border within 1 μm of the nucleus). EEA1 structures contacting cortactin were defined as EEA1 surfaces with a shortest distance to a cortactin surface with a value of zero. The EEA1 structures that contacted cortactin were represented as a percentage of the total number of EEA1 structures.

Ciliogenesis assay

To induce ciliogenesis, mock- and FCHSD2 siRNA-treated RPE-1 cells were shifted to starvation media (DMEM/F12, 0.2% FBS, 1% penicillin-streptomycin, 2 mM L-Glutamine, 1X non-essential amino acids) for 4 h at 37°C in 5% CO_2. Cells were then rinsed once with cold PBS and fixed with 100% methanol at −20°C for 5 min. After fixation, coverslips were washed three times with PBS, and a prestaining incubation was performed for 30 min (0.5% Triton X and 0.5% BSA in PBS). Coverslips were costained with primary anti-CP110 and anti-acetylated-tubulin antibodies for 1 h at room temperature. The coverslips were subsequently washed three times and stained with the appropriate fluorochrome-conjugated secondary antibodies. Following secondary incubation, the coverslips were washed three times with PBS and mounted in Fluoromount. Images were taken using a Zeiss LSM 800 confocal microscope (Carl Zeiss) with a 63 ×/1.4 NA oil objective, and maximal intensity orthogonal projections were obtained and quantified in the Zen Blue software. The number of ciliated and non-ciliated cells was manually counted. Ciliated cells were considered to have an elongated acetylated tubulin stain along with retention of CP110 on one of the two centrioles. Nonciliated cells typically retained CP110 on both centrioles. The percentage of ciliated cells from the total number of cells was quantified for each image and plotted.

Statistical analysis

Data for all experiments were collected from three independent experiments and graphed with the mean and SD. Normality was determined with a D'Agostino and Pearson (or Shapiro–Wilk) normality test. If the normal distribution assumption was met, an unpaired two-tailed *t* test was used to assess *p*-values and determine statistical significance between two groups ($p < 0.05$). In the event that the distribution did not meet the assumption of normality, a Mann–Whitney nonparametric two-tailed test was used to assess significance. All the graphical and statistical tests were done using GraphPad Prism 10.2.3.

Data availability

No data from this manuscript require deposition in a public database.

ACKNOWLEDGMENTS

This work was supported by NIH grant R35GM144102 from the National Institute of General Medical Sciences (S.C.), and by NIH T32 training grant CA009476 (Cancer Biology Training Program; D.F.), and by the Research Council of Finland (Research Fellow; L.A.-S.).

REFERENCES

Almeida-Souza L, Frank RAW, Garcia-Nafria J, Colussi A, Gunawardana N, Johnson CM, Yu M, Howard G, Andrews B, Vallis Y, *et al*. (2018). A flat BAR protein promotes actin polymerization at the base of clathrin-coated pits. Cell 174, 325–337.e314.

Anitei M, Hoflack B (2011). Bridging membrane and cytoskeleton dynamics in the secretory and endocytic pathways. Nat Cell Biol 14, 11–19.

Bai M, Pang X, Lou J, Zhou Q, Zhang K, Ma J, Li J, Sun F, Hsu VW (2012). Mechanistic insights into regulated cargo binding by ACAP1 protein. J Biol Chem 287, 28675–28685.

Bales KL, Gross AK (2016). Aberrant protein trafficking in retinal degenerations: The initial phase of retinal remodeling. Exp Eye Res 150, 71–80.

Becalska AN, Kelley CF, Berciu C, Stanishneva-Konovalova TB, Fu X, Wang S, Sokolova OS, Nicastro D, Rodal AA (2013). Formation of membrane ridges and scallops by the F-BAR protein Nervous Wreck. Mol Biol Cell 24, 2406–2418.

Blanchette CR, Scalera AL, Harris KP, Zhao Z, Dresselhaus EC, Koles K, Yeh A, Apiki JK, Stewart BA, Rodal AA (2022). Local regulation of extracellular vesicle traffic by the synaptic endocytic machinery. J Cell Biol 221, e202112094.

Bruck S, Huber TB, Ingham RJ, Kim K, Niederstrasser H, Allen PM, Pawson T, Cooper JA, Shaw AS (2006). Identification of a novel inhibitory actin-capping protein binding motif in CD2-associated protein. J Biol Chem 281, 19196–19203.

Burd C, Cullen PJ (2014). Retromer: A master conductor of endosome sorting. Cold Spring Harb Perspect Biol 6, a016774.

Cai B, Caplan S, Naslavsky N (2012). cPLA2alpha and EHD1 interact and regulate the vesiculation of cholesterol-rich, GPI-anchored, protein-containing endosomes. Mol Biol Cell 23, 1874–1888.

Cai B, Giridharan SS, Zhang J, Saxena S, Bahl K, Schmidt JA, Sorgen PL, Guo W, Naslavsky N, Caplan S (2013). Differential roles of C-terminal Eps15 homology domain proteins as vesiculators and tubulators of recycling endosomes. J Biol Chem 288, 30172–30180.

Cai B, Xie S, Caplan S, Naslavsky N (2014). GRAF1 forms a complex with MICAL-L1 and EHD1 to cooperate in tubular recycling endosome vesiculation. Front Cell Dev Biol 2, 22.

Caswell P, Norman J (2008). Endocytic transport of integrins during cell migration and invasion. Trends Cell Biol 18, 257–263.

Cooper JA, Pollard TD (1985). Effect of capping protein on the kinetics of actin polymerization. Biochemistry 24, 793–799.

Courtellemont T, De Leo MG, Gopaldass N, Mayer A (2022). CROP: a retromer-PROPPIN complex mediating membrane fission in the endo-lysosomal system. EMBO J 41, e109646.

Coyle IP, Koh YH, Lee WC, Slind J, Fergestad T, Littleton JT, Ganetzky B (2004). Nervous wreck, an SH3 adaptor protein that interacts with Wsp, regulates synaptic growth in Drosophila. Neuron 41, 521–534.

Cullen PJ, Steinberg F (2018). To degrade or not to degrade: mechanisms and significance of endocytic recycling. Nat Rev Mol Cell Biol 19, 679–696.

Dai J, Li J, Bos E, Porcionatto M, Premont RT, Bourgoin S, Peters PJ, Hsu VW (2004). ACAP1 promotes endocytic recycling by recognizing recycling sorting signals. Dev Cell 7, 771–776.

Del Signore SJ, Kelley CF, Messelaar EM, Lemos T, Marchan MF, Ermanoska B, Mund M, Fai TG, Kaksonen M, Rodal AA (2021). An autoinhibitory clamp of actin assembly constrains and directs synaptic endocytosis. Elife 10, e69597.

Delevoye C, Heiligenstein X, Ripoll L, Gilles-Marsens F, Dennis MK, Linares RA, Derman L, Gokhale A, Morel E, Faundez V, *et al*. (2016). BLOC-1 brings together the actin and microtubule cytoskeletons to generate recycling endosomes. Curr Biol 26, 1–13.

Deo R, Kushwah MS, Kamerkar SC, Kadam NY, Dar S, Babu K, Srivastava A, Pucadyil TJ (2018). ATP-dependent membrane remodeling links EHD1 functions to endocytic recycling. Nat Commun 9, 5187.

Derivery E, Helfer E, Henriot V, Gautreau A (2012). Actin polymerization controls the organization of WASH domains at the surface of endosomes. PLoS One 7, e39774.

Derivery E, Sousa C, Gautier JJ, Lombard B, Loew D, Gautreau A (2009). The Arp2/3 activator WASH controls the fission of endosomes through a large multiprotein complex. Dev Cell 17, 712–723.

Dharmalingam E, Haeckel A, Pinyol R, Schwintzer L, Koch D, Kessels MM, Qualmann B (2009). F-BAR proteins of the syndapin family shape the plasma membrane and are crucial for neuromorphogenesis. J Neurosci 29, 13315–13327.

Dhawan K, Naslavsky N, Caplan S (2020). Sorting nexin 17 (SNX17) links endosomal sorting to Eps15 homology domain protein 1 (EHD1)-mediated fission machinery. J Biol Chem 295, 3837–3850.

Dhawan K, Naslavsky N, Caplan S (2022). Coronin2A links actin-based endosomal processes to the EHD1 fission machinery. Mol Biol Cell 33, ar107.

Farmer T, Xie S, Naslavsky N, Stockli J, James DE, Caplan S (2021). Defining the protein and lipid constituents of tubular recycling endosomes. J Biol Chem 296, 100190.

Giridharan SS, Cai B, Naslavsky N, Caplan S (2012). Trafficking cascades mediated by Rab35 and its membrane hub effector, MICAL-L1. Commun Integr Biol 5, 384–387.

Giridharan SS, Cai B, Vitale N, Naslavsky N, Caplan S (2013). Cooperation of MICAL-L1, syndapin2, and phosphatidic acid in tubular recycling endosome biogenesis. Mol Biol Cell 24, 1776–1790, S1–S15.

Gomez TS, Billadeau DD (2009). A FAM21-containing WASH complex regulates retromer-dependent sorting. Dev Cell 17, 699–711.

Gopaldass N, Chen KE, Collins B, Mayer A (2024). Assembly and fission of tubular carriers mediating protein sorting in endosomes. Nat Rev Mol Cell Biol 25, 765–783.

Gopaldass N, Fauvet B, Lashuel H, Roux A, Mayer A (2017). Membrane scission driven by the PROPPIN Atg18. EMBO J 36, 3274–3291.
Grassart A, Cheng AT, Hong SH, Zhang F, Zenzer N, Feng Y, Briner DM, Davis GD, Malkov D, Drubin DG (2014). Actin and dynamin2 dynamics and interplay during clathrin-mediated endocytosis. J Cell Biol 205, 721–735.
Gubar O, Croise P, Kropyvko S, Gryaznova T, Toth P, Blangy A, Vitale N, Rynditch A, Gasman S, Ory S (2020). The atypical Rho GTPase RhoU interacts with intersectin-2 to regulate endosomal recycling pathways. J Cell Sci 133, jcs234104.
Haberg K, Lundmark R, Carlsson SR (2008). SNX18 is an SNX9 paralog that acts as a membrane tubulator in AP-1-positive endosomal trafficking. J Cell Sci 121, 1495–1505.
Harbour ME, Breusegem SY, Seaman MN (2012). Recruitment of the endosomal WASH complex is mediated by the extended 'tail' of Fam21 binding to the retromer protein Vps35. Biochem J 442, 209–220.
Havrylov S, Rzhepetskyy Y, Malinowska A, Drobot L, Redowicz MJ (2009). Proteins recruited by SH3 domains of Ruk/CIN85 adaptor identified by LC-MS/MS. Proteome Sci 7, 21.
Hoffman HK, Prekeris R (2022). Roles of the actin cytoskeleton in ciliogenesis. J Cell Sci 135, jcs259030.
Hoyer MJ, Chitwood PJ, Ebmeier CC, Striepen JF, Qi RZ, Old WM, Voeltz GK (2018). A novel class of ER membrane proteins regulates ER-associated endosome fission. Cell 175, 254–265.e214.
Hsu VW, Bai M, Li J (2012). Getting active: Protein sorting in endocytic recycling. Nat Rev Mol Cell Biol 13, 323–328.
Huttlin EL, Bruckner RJ, Navarrete-Perea J, Cannon JR, Baltier K, Gebreab F, Gygi MP, Thornock A, Zarraga G, Tam S, *et al.* (2021). Dual proteome-scale networks reveal cell-specific remodeling of the human interactome. Cell 184, 3022–3040.e3028.
Huttlin EL, Bruckner RJ, Paulo JA, Cannon JR, Ting L, Baltier K, Colby G, Gebreab F, Gygi MP, Parzen H, *et al.* (2017). Architecture of the human interactome defines protein communities and disease networks. Nature 545, 505–509.
Ioannou MS, Kulasekaran G, Fotouhi M, Morein JJ, Han C, Tse S, Nossova N, Han T, Mannard E, McPherson PS (2017). Intersectin-s interaction with DENND2B facilitates recycling of epidermal growth factor receptor. EMBO Rep 18, 2119–2130.
Jethwa N, Chung GH, Lete MG, Alonso A, Byrne RD, Calleja V, Larijani B (2015). Endomembrane PtdIns(3,4,5)P3 activates the PI3K-Akt pathway. J Cell Sci 128, 3456–3465.
Jia D, Gomez TS, Billadeau DD, Rosen MK (2012). Multiple repeat elements within the FAM21 tail link the WASH actin regulatory complex to the retromer. Mol Biol Cell 23, 2352–2361.
Jones T, Naslavsky N, Caplan S (2020). Eps15 Homology Domain Protein 4 (EHD4) is required for Eps15 Homology Domain Protein 1 (EHD1)-mediated endosomal recruitment and fission. PLoS One 15, e0239657.
Kamerkar SC, Roy K, Bhattacharyya S, Pucadyil TJ (2019). A screen for membrane fission catalysts identifies the ATPase EHD1. Biochemistry 58, 65–71.
Kelley CF, Messelaar EM, Eskin TL, Wang S, Song K, Vishnia K, Becalska AN, Shupliakov O, Hagan MF, Danino D, *et al.* (2015). Membrane charge directs the outcome of F-BAR domain lipid binding and autoregulation. Cell Rep 13, 2597–2609.
Kessels MM, Qualmann B (2002) Syndapins integrate N-WASP in receptor-mediated endocytosis. EMBO J 21, 6083–6094.
Li J, Ballif BA, Powelka AM, Dai J, Gygi SP, Hsu VW (2005). Phosphorylation of ACAP1 by Akt regulates the stimulation-dependent recycling of integrin beta1 to control cell migration. Dev Cell 9, 663–673.
Madhivanan K, Aguilar RC (2014). Ciliopathies: the trafficking connection. Traffic 15, 1031–1056.
McConnell P, Mekel M, Kozlov AG, Mooren OL, Lohman TM, Cooper JA (2020). Comparative analysis of CPI-motif regulation of biochemical functions of actin capping protein. Biochemistry 59, 1202–1215.
McNally KE, Cullen PJ (2018). Endosomal retrieval of cargo: Retromer is not alone. Trends Cell Biol 28, 807–822.
McNally KE, Faulkner R, Steinberg F, Gallon M, Ghai R, Pim D, Langton P, Pearson N, Danson CM, Nagele H, *et al.* (2017). Retriever is a multiprotein complex for retromer-independent endosomal cargo recycling. Nat Cell Biol 19, 1214–1225.
Merrifield CJ, Feldman ME, Wan L, Almers W (2002). Imaging actin and dynamin recruitment during invagination of single clathrin-coated pits. Nat Cell Biol 4, 691–698.
Merrifield CJ, Qualmann B, Kessels MM, Almers W (2004). Neural Wiskott Aldrich Syndrome Protein (N-WASP) and the Arp2/3 complex are recruited to sites of clathrin-mediated endocytosis in cultured fibroblasts. Eur J Cell Biol 83, 13–18.
Muriel O, Tomas A, Scott CC, Gruenberg J (2016). Moesin and cortactin control actin-dependent multivesicular endosome biogenesis. Mol Biol Cell 27, 3305–3316.
Naslavsky N, Caplan S (2011). EHD proteins: key conductors of endocytic transport. Trends Cell Biol 21, 122–131.
Naslavsky N, Caplan S (2018). The enigmatic endosome - sorting the ins and outs of endocytic trafficking. J Cell Sci 131, jcs216499.
Naslavsky N, Caplan S (2023a). Advances and challenges in understanding endosomal sorting and fission. FEBS J 290, 4187–4195.
Naslavsky N, Caplan S (2023b). Receptor-mediated internalization promotes increased endosome size and number in a RAB4- and RAB5-dependent manner. Eur J Cell Biol 102, 151339.
Nolen BJ, Tomasevic N, Russell A, Pierce DW, Jia Z, McCormick CD, Hartman J, Sakowicz R, Pollard TD (2009). Characterization of two classes of small molecule inhibitors of Arp2/3 complex. Nature 460, 1031–1034.
O'Connor-Giles KM, Ho LL, Ganetzky B (2008). Nervous wreck interacts with thickveins and the endocytic machinery to attenuate retrograde BMP signaling during synaptic growth. Neuron 58, 507–518.
Ohno H, Hirabayashi S, Kansaku A, Yao I, Tajima M, Nishimura W, Ohnishi H, Mashima H, Fujita T, Omata M, *et al.* (2003). Carom: a novel membrane-associated guanylate kinase-interacting protein with two SH3 domains. Oncogene 22, 8422–8431.
Pedersen LB, Mogensen JB, Christensen ST (2016). Endocytic control of cellular signaling at the primary cilium. Trends Biochem Sci 41, 784–797.
Piotrowski JT, Gomez TS, Schoon RA, Mangalam AK, Billadeau DD (2013). WASH knockout T cells demonstrate defective receptor trafficking, proliferation, and effector function. Mol Cell Biol 33, 958–973.
Pollard TD (2007). Regulation of actin filament assembly by Arp2/3 complex and formins. Annu Rev Biophys Biomol Struct 36, 451–477.
Puthenveedu MA, Lauffer B, Temkin P, Vistein R, Carlton P, Thorn K, Taunton J, Weiner OD, Parton RG, von Zastrow M (2010). Sequence-dependent sorting of recycling proteins by actin-stabilized endosomal microdomains. Cell 143, 761–773.
Qualmann B, Kelly RB (2000). Syndapin isoforms participate in receptor-mediated endocytosis and actin organization. J Cell Biol 148, 1047–1062.
Qualmann B, Roos J, DiGregorio PJ, Kelly RB (1999). Syndapin I, a synaptic dynamin-binding protein that associates with the neural Wiskott-Aldrich syndrome protein. Mol Biol Cell 10, 501–513.
Rahajeng J, Giridharan SS, Cai B, Naslavsky N, Caplan S (2012). MICAL-L1 is a tubular endosomal membrane hub that connects Rab35 and Arf6 with Rab8a. Traffic 13, 82–93.
Rahajeng J, Giridharan SS, Naslavsky N, Caplan S (2010). Collapsin response mediator protein-2 (Crmp2) regulates trafficking by linking endocytic regulatory proteins to dynein motors. J Biol Chem 285, 31918–31922.
Roberts RL, Barbieri MA, Pryse KM, Chua M, Morisaki JH, Stahl PD (1999). Endosome fusion in living cells overexpressing GFP-rab5. J Cell Sci 112, 3667–3675.
Rodal AA, Blunk AD, Akbergenova Y, Jorquera RA, Buhl LK, Littleton JT (2011). A presynaptic endosomal trafficking pathway controls synaptic growth signaling. J Cell Biol 193, 201–217.
Rodal AA, Motola-Barnes RN, Littleton JT (2008). Nervous wreck and Cdc42 cooperate to regulate endocytic actin assembly during synaptic growth. J Neurosci 28, 8316–8325.
Roux A, Uyhazi K, Frost A, De Camilli P (2006). GTP-dependent twisting of dynamin implicates constriction and tension in membrane fission. Nature 441, 528–531.
Rowland AA, Chitwood PJ, Phillips MJ, Voeltz GK (2014). ER contact sites define the position and timing of endosome fission. Cell 159, 1027–1041.
Seaman MN, Gautreau A, Billadeau DD (2013). Retromer-mediated endosomal protein sorting: all WASHed up! Trends Cell Biol 23, 522–528.
Sengar AS, Wang W, Bishay J, Cohen S, Egan SE (1999). The EH and SH3 domain Ese proteins regulate endocytosis by linking to dynamin and Eps15. EMBO J 18, 1159–1171.
Sharma M, Giridharan SS, Rahajeng J, Caplan S, Naslavsky N (2010). MICAL-L1: An unusual Rab effector that links EHD1 to tubular recycling endosomes. Commun Integr Biol 3, 181–183.
Sharma M, Giridharan SS, Rahajeng J, Naslavsky N, Caplan S (2009). MICAL-L1 links EHD1 to tubular recycling endosomes and regulates receptor recycling. Mol Biol Cell 20, 5181–5194.

Shi R, Shi X, Qin D, Tang S, Vermeulen M, Zhang X (2021). SNX27-driven membrane localisation of OTULIN antagonises linear ubiquitination and NF-kappaB signalling activation. Cell Biosci 11, 146.
Simonetti B, Cullen PJ (2019). Actin-dependent endosomal receptor recycling. Curr Opin Cell Biol 56, 22–33.
Solinger JA, Spang A (2022). Sorting of cargo in the tubular endosomal network. Bioessays 44, e2200158.
Stanishneva-Konovalova TB, Kelley CF, Eskin TL, Messelaar EM, Wasserman SA, Sokolova OS, Rodal AA (2016). Coordinated autoinhibition of F-BAR domain membrane binding and WASp activation by Nervous Wreck. Proc Natl Acad Sci USA 113, E5552–5561.
Steinberg F, Gallon M, Winfield M, Thomas EC, Bell AJ, Heesom KJ, Tavare JM, Cullen PJ (2013). A global analysis of SNX27-retromer assembly and cargo specificity reveals a function in glucose and metal ion transport. Nat Cell Biol 15, 461–471.
Stenmark H, Parton RG, Steele-Mortimer O, Lutcke A, Gruenberg J, Zerial M (1994). Inhibition of rab5 GTPase activity stimulates membrane fusion in endocytosis. EMBO J 13, 1287–1296.
Temkin P, Lauffer B, Jager S, Cimermancic P, Krogan NJ, von Zastrow M (2011). SNX27 mediates retromer tubule entry and endosome-to-plasma membrane trafficking of signalling receptors. Nat Cell Biol 13, 715–721.
Wang E, Brown PS, Aroeti B, Chapin SJ, Mostov KE, Dunn KW (2000). Apical and basolateral endocytic pathways of MDCK cells meet in acidic common endosomes distinct from a nearly-neutral apical recycling endosome. Traffic 1, 480–493.
Wang H, Zhao D, Du H, Zhai X, Wu S, Lin L, Xu Z, Lu Q (2022). Deafness-related protein PDZD7 forms complex with the C-terminal tail of FCHSD2. Biochem J 479, 1393–1405.
Wang J, Fedoseienko A, Chen B, Burstein E, Jia D, Billadeau DD (2018). Endosomal receptor trafficking: Retromer and beyond. Traffic 19, 578–590.
Wang Q, Navarro MV, Peng G, Molinelli E, Goh SL, Judson BL, Rajashankar KR, Sondermann H (2009). Molecular mechanism of membrane constriction and tubulation mediated by the F-BAR protein Pacsin/Syndapin. Proc Natl Acad Sci USA 106, 12700–12705.
Wong KA, Wilson J, Russo A, Wang L, Okur MN, Wang X, Martin NP, Scappini E, Carnegie GK, O'Bryan JP (2012). Intersectin (ITSN) family of scaffolds function as molecular hubs in protein interaction networks. PLoS One 7, e36023.
Xiao GY, Mohanakrishnan A, Schmid SL (2018). Role for ERK1/2-dependent activation of FCHSD2 in cancer cell-selective regulation of clathrin-mediated endocytosis. Proc Natl Acad Sci USA 115, E9570–E9579.
Xiao GY, Schmid SL (2020). FCHSD2 controls oncogenic ERK1/2 signaling outcome by regulating endocytic trafficking. PLoS Biol 18, e3000778.
Xie S, Bahl K, Reinecke JB, Hammond GR, Naslavsky N, Caplan S (2016). The endocytic recycling compartment maintains cargo segregation acquired upon exit from the sorting endosome. Mol Biol Cell 27, 108–126.
Xie S, Farmer T, Naslavsky N, Caplan S (2019). MICAL-L1 coordinates ciliogenesis by recruiting EHD1 to the primary cilium. J Cell Sci 132, jcs233973.
Xie S, Naslavsky N, Caplan S (2023). EHD1 promotes CP110 ubiquitination by centriolar satellite delivery of HERC2 to the mother centriole. EMBO Rep 24, e56317.
Xu Y, Xia J, Liu S, Stein S, Ramon C, Xi H, Wang L, Xiong X, Zhang L, He D, *et al*. (2017). Endocytosis and membrane receptor internalization: implication of F-BAR protein Carom. Front Biosci (Landmark Ed) 22, 1439–1457.
Zech T, Calaminus SD, Caswell P, Spence HJ, Carnell M, Insall RH, Norman J, Machesky LM (2011). The Arp2/3 activator WASH regulates alpha5beta1-integrin-mediated invasive migration. J Cell Sci 124, 3753–3759.
Zhai X, Du H, Shen Y, Zhang X, Chen Z, Wang Y, Xu Z (2022a). FCHSD2 is required for stereocilia maintenance in mouse cochlear hair cells. J Cell Sci 135, jcs259912.
Zhai X, Shen Y, Zhang X, Li T, Lu Q, Xu Z (2022b). FCHSD2 cooperates with CDC42 and N-WASP to regulate cell protrusion formation. Biochim Biophys Acta Mol Cell Res 1869, 119134.
Zhao J, Bruck S, Cemerski S, Zhang L, Butler B, Dani A, Cooper JA, Shaw AS (2013). CD2AP links cortactin and capping protein at the cell periphery to facilitate formation of lamellipodia. Mol Cell Biol 33, 38–47.